

PREPARATION AND OPERATIONS OF THE MISSION PERFORMANCE  
CENTRE (MPC) FOR THE COPERNICUS SENTINEL-3 MISSION

**S3-A OLCI Cyclic Performance Report**

**Cycle No. 017**

**Start date: 21/04/2017**

**End date: 18/05/2017**



*Mission  
Performance  
Centre*



**Ref.:** S3MPC.ACR.PR.01-017  
**Issue:** 1.0  
**Date:** 24/05/2017  
**Contract:** 4000111836/14/I-LG

<b>Customer:</b> ESA	<b>Document Ref.:</b> S3MPC.ACR.PR.01-017
<b>Contract No.:</b> 4000111836/14/I-LG	<b>Date:</b> 24/05/2017
	<b>Issue:</b> 1.0

<b>Project:</b>	PREPARATION AND OPERATIONS OF THE MISSION PERFORMANCE CENTRE (MPC) FOR THE COPERNICUS SENTINEL-3 MISSION		
<b>Title:</b>	S3-A OLCI Cyclic Performance Report		
<b>Author(s):</b>	OLCI ESLs		
<b>Approved by:</b>	L. Bourg, OLCI ESL Coordinator	<b>Authorized by</b>	Frédéric Rouffi, OPT Technical Performance Manager
<b>Distribution:</b>	ESA, EUMETSAT, S3MPC consortium		
<b>Accepted by ESA</b>	S. Dransfeld, MPC Deputy TO for OPT  P. Féménias, MPC TO		
<b>Filename</b>	S3MPC.ACR.PR.01-017 - i1r0 - OLCI Cyclic Report 017.docx		

#### Disclaimer

The work performed in the frame of this contract is carried out with funding by the European Union. The views expressed herein can in no way be taken to reflect the official opinion of either the European Union or the European Space Agency.







**Sentinel-3 MPC**  
**S3-A OLCI Cyclic Performance Report**  
**Cycle No. 017**

Ref.: S3MPC.ACR.PR.01-017  
 Issue: 1.0  
 Date: 24/05/2017  
 Page: iv

## Table of content

<b>TABLE OF CONTENT .....</b>	<b>IV</b>
<b>LIST OF FIGURES .....</b>	<b>V</b>
<b>1 INSTRUMENT MONITORING .....</b>	<b>1</b>
1.1 CCD TEMPERATURES.....	1
1.2 RADIOMETRIC CALIBRATION .....	2
1.2.1 <i>Dark Offsets [OLCI-L1B-CV-230]</i> .....	4
1.2.2 <i>Instrument response and degradation modelling [OLCI-L1B-CV-250]</i> .....	7
1.2.3 <i>Ageing of nominal diffuser [OLCI-L1B-CV-240]</i> .....	18
1.2.4 <i>Updating of calibration ADF [OLCI-L1B-CV-260]</i> .....	22
1.2.5 <i>Radiometric Calibrations for sun azimuth angle dependency and Yaw Manoeuvres for Solar Diffuser on-orbit re-characterization [OLCI-L1B-CV-270 and OLCI-L1B-CV-280]</i> .....	23
1.3 SPECTRAL CALIBRATION [OLCI-L1B-CV-400].....	23
1.4 SIGNAL TO NOISE ASSESSMENT [OLCI-L1B-CV-620] .....	23
1.4.1 <i>SNR from Radiometric calibration data</i> .....	23
1.4.2 <i>SNR from EO data</i> .....	25
1.5 GEOMETRIC CALIBRATION/VALIDATION .....	25
<b>2 OLCI LEVEL 1 PRODUCT VALIDATION .....</b>	<b>28</b>
<b>3 LEVEL 2 LAND PRODUCTS VALIDATION .....</b>	<b>33</b>
<b>4 LEVEL 2 WATER PRODUCTS VALIDATION .....</b>	<b>36</b>
<b>5 LEVEL 2 SYN PRODUCTS VALIDATION.....</b>	<b>43</b>
<b>6 EVENTS .....</b>	<b>44</b>
<b>7 APPENDIX A .....</b>	<b>45</b>

	<p><b>Sentinel-3 MPC</b></p> <p><b>S3-A OLCI Cyclic Performance Report</b></p> <p><b>Cycle No. 017</b></p>	<p>Ref.: S3MPC.ACR.PR.01-017</p> <p>Issue: 1.0</p> <p>Date: 24/05/2017</p> <p>Page: v</p>
--	--	---

## List of Figures

Figure 1: long term monitoring of CCD temperatures using minimum value (top), time averaged values (middle), and maximum value (bottom) provided in the annotations of the Radiometric Calibration Level 1 products, for the Shutter frames, all radiometric calibrations so far. ----- 1

Figure 2: Same as Figure 1 for diffuser frames. ----- 2

Figure 3: Sun azimuth angles during acquired Radiometric Calibrations (diffuser frame) on top of nominal yearly cycle (black curve). Diffuser 1 with diamonds, diffuser 2 with crosses, 2016 acquisitions in blue, 2017 in red. ----- 3

Figure 4: Sun geometry during radiometric Calibrations on top of characterization ones (diffuser frame) 3

Figure 5: Dark Offset for band Oa1 (top) and Oa21 (bottom), all radiometric calibrations so far except the first one (orbit 183) for which the instrument was not thermally stable yet. ----- 4

Figure 6: map of periodic noise for the 5 cameras, for band Oa21. X-axis is detector number (East part, from 540 to 740, where the periodic noise occurs), Y-axis is the orbit number. The counts have been corrected from the west detectors mean value (not affected by periodic noise). Periodic noise amplitude is high in camera 2, 3 and 4. It is lower in camera 4 and small in camera 1. ----- 5

Figure 7: Dark Current for band Oa1 (top) and Oa21 (bottom), all radiometric calibrations so far except the first one (orbit 183) for which the instrument was not thermally stable yet. ----- 6

Figure 8: left column: ACT mean on 400 first detectors of Dark Current coefficients for spectral band Oa01 (top) and Oa21 (bottom). Right column: same as left column but for Standard deviation instead of mean. We see an increase of the DC level as a function of time especially for band Oa21. A possible explanation could be the increase of the number of hot pixels which is more important in Oa21 because this band is made of more CCD lines than band Oa01 and thus receives more cosmic rays impacts. It is known that cosmic rays degrade the structure of the CCD, generating more and more hot pixels at long term scales. ----- 6

Figure 9: Gain Coefficients for band Oa1 (top) and Oa21 (bottom), all diffuser 1 radiometric calibrations so far except the first one (orbit 183) for which the instrument was not thermally stable yet. ----- 7

Figure 10: time evolution of the camera-averaged Absolute gain coefficients for bands Oa1, Oa7, Oa14 and Oa21 (from left to right and top to bottom). ----- 8

Figure 11: camera averaged gain relative evolution with respect to “best geometry” calibration (22/11), as a function of elapsed time since first calibration acquired after the fix of the Start Trackers issue; one curve for each band (see colour code on plots), one plot for each module. ----- 9

Figure 12: Across-track profiles of Gains relative evolution with respect to “best geometry” calibration over a relatively large time distance (from -34 to +12 weeks) and for varying geometries, more or less symmetrical with respect to reference one: on the right column time distance remains almost constant around 2 weeks, as calibrations compared to reference are selected within the Yaw Manoeuvres with SAA differences of -6.6, 0 and 5.6 degrees from top to bottom, the left column shows the comparisons at equal or close  $\delta$ SAA than right column, but as large as possible time distance.(from top to bottom

	<b>Sentinel-3 MPC</b> <b>S3-A OLCI Cyclic Performance Report</b> <b>Cycle No. 017</b>	Ref.: S3MPC.ACR.PR.01-017 Issue: 1.0 Date: 24/05/2017 Page: vi
--	---	---

time differences are respectively +12,-34 and +22.8 weeks). Influence of geometry and time are both clearly visible and can be distinguished from each other.-----10

Figure 13: same as Figure 11 after normalization by band Oa18. -----11

Figure 14: same as Figure 12 after normalization by band Oa18. -----12

Figure 15: same as Figure 11 but using the updated BRDF model. The data have NOT been normalized by band Oa18. The star tracker anomaly fix is represented by a vertical red dashed line.-----13

Figure 16: Camera-averaged instrument evolution since channel programming change (25/04/2016) and up to most recent calibration (12/05/2017) versus wavelength.-----14

Figure 17: For the 5 cameras: Evolution model performance, as camera-average and standard deviation of ratio of Model over Data vs. wavelength, for each orbit of the test dataset, including 3 calibration in extrapolation, with a colour code for each calibration from blue (oldest) to red (most recent).-----15

Figure 18: model performance: ratio of model over data for all pixels (x axis) of all orbits (y axis), for channel Oa4. The outlying orbit #40 is that of 31/03/2017. -----16

Figure 19: Evolution model performance, as ratio of Model over Data vs. pixels, all cameras side by side, over the whole current calibration dataset (since instrument programming update), including 7 calibration in extrapolation, channels Oa1 to Oa6. -----16

Figure 20: same as Figure 19 for channels Oa7 to Oa14. -----17

Figure 21: same as Figure 19 for channels Oa15 to Oa21.-----18

Figure 22: diffuser 1 ageing for spectral band Oa01. We see strong ACT low frequency structures that are due to residual of BRDF modelling. -----19

Figure 23: same as Figure 22 for spectral band Oa16. We use this band in order to normalize other bands and remove the ACT structures due to residual of BRDF modelling. Normalized curve for spectral band Oa01 is presented in Figure 24. -----20

Figure 24: same as Figure 22 after normalization by band Oa16. Ageing of the diffuser 1 is now visible in the 5 cameras.-----20

Figure 25: Diffuser 1 ageing as a function of wavelength (or spectral band). Ageing is visible in spectral band #1 to #5. -----21

Figure 26: Camera averaged ageing (normalized by band Oa16) as a function of time. Linear fit for each camera is plotted. The slope (% loss per year) and the correlation coefficient of the linear fits are written in the legend at the bottom. -----22

Figure 27: Signal to Noise ratio as a function of the spectral band for the 5 cameras. These results have been computed from radiometric calibration data. All calibrations except first one (orbit 183) are presents with the colours corresponding to the orbit number (see legend). The SNR is very stable with time: the curves for all orbits are almost superimposed. The dashed curve is the ESA requirement. -----24

Figure 28: long-term stability of the SNR estimates from Calibration data, example of channel Oa1. -----25

Figure 29: histograms of geolocation errors for the along-track (left) and across-track (right) directions.26

	<p><b>Sentinel-3 MPC</b></p> <p><b>S3-A OLCI Cyclic Performance Report</b></p> <p><b>Cycle No. 017</b></p>	<p>Ref.: S3MPC.ACR.PR.01-017</p> <p>Issue: 1.0</p> <p>Date: 24/05/2017</p> <p>Page: vii</p>
--	--	---

Figure 30: georeferencing error in along-track (left) and across-track (right) directions for all the GCPs. 26

Figure 31: same as Figure 30 for 23<sup>rd</sup> and 24<sup>th</sup> of April, with a restricted vertical scale. -----27

Figure 32: same as Figure 30 for 3<sup>rd</sup> and 4<sup>th</sup> of May, with a restricted vertical scale. -----27

Figure 33: same as Figure 30 for 14<sup>th</sup> and 15<sup>th</sup> of May, with a restricted vertical scale. -----27

Figure 34: summary of S3ETRAC products generation for OLCI (number of OLCI L1 products Ingested, yellow – number of S3ETRAC extracted products generated, blue – number of S3ETRAC runs without generation of output product (data not meeting selection requirements), green – number of runs ending in error, red, one plot per site type). -----29

Figure 35: Time-series of the elementary ratios (observed/simulated) signal from S3A/OLCI for (top) band Oa8 and (bottom) band Oa17 over Six PICS Cal/Val sites. Dashed-green and orange lines indicate the 2% and 5% respectively. Error bars indicate the desert methodology uncertainty. -----30

Figure 36: The estimated gain values for S3A/OLCI over the 6 PICS sites identified by CEOS over the period September 2016 – May 2017 as a function of wavelength. Dashed-green and orange lines indicate the 2% and 5% respectively. Error bars indicate the desert methodology uncertainty. -----31

Figure 37: The estimated gain values for S3A/OLCI from Glint, Rayleigh, and PICS over the period September 2016 – May 2017 as a function of wavelength. We use the gain value of Oa8 from Desert method as reference gain for Glint. Dashed-green and orange lines indicate the 2% and 5% respectively. Error bars indicate the methods uncertainties. -----32

Figure 38 Oscar Rayleigh results for February 2017 for AtIN, IndS, PacN and PacSE sites. -----32



## 1 Instrument monitoring

### 1.1 CCD temperatures

The monitoring of the CCD temperatures is based on MPMF data extractions not yet operational. In the meantime, we monitor the CCD temperatures on the long-term using Radiometric Calibration Annotations (see Figure 1). Variations are very small (0.08 C peak-to-peak) and no trend can be identified. Data from current cycle (rightmost data points) do not show any specificity.

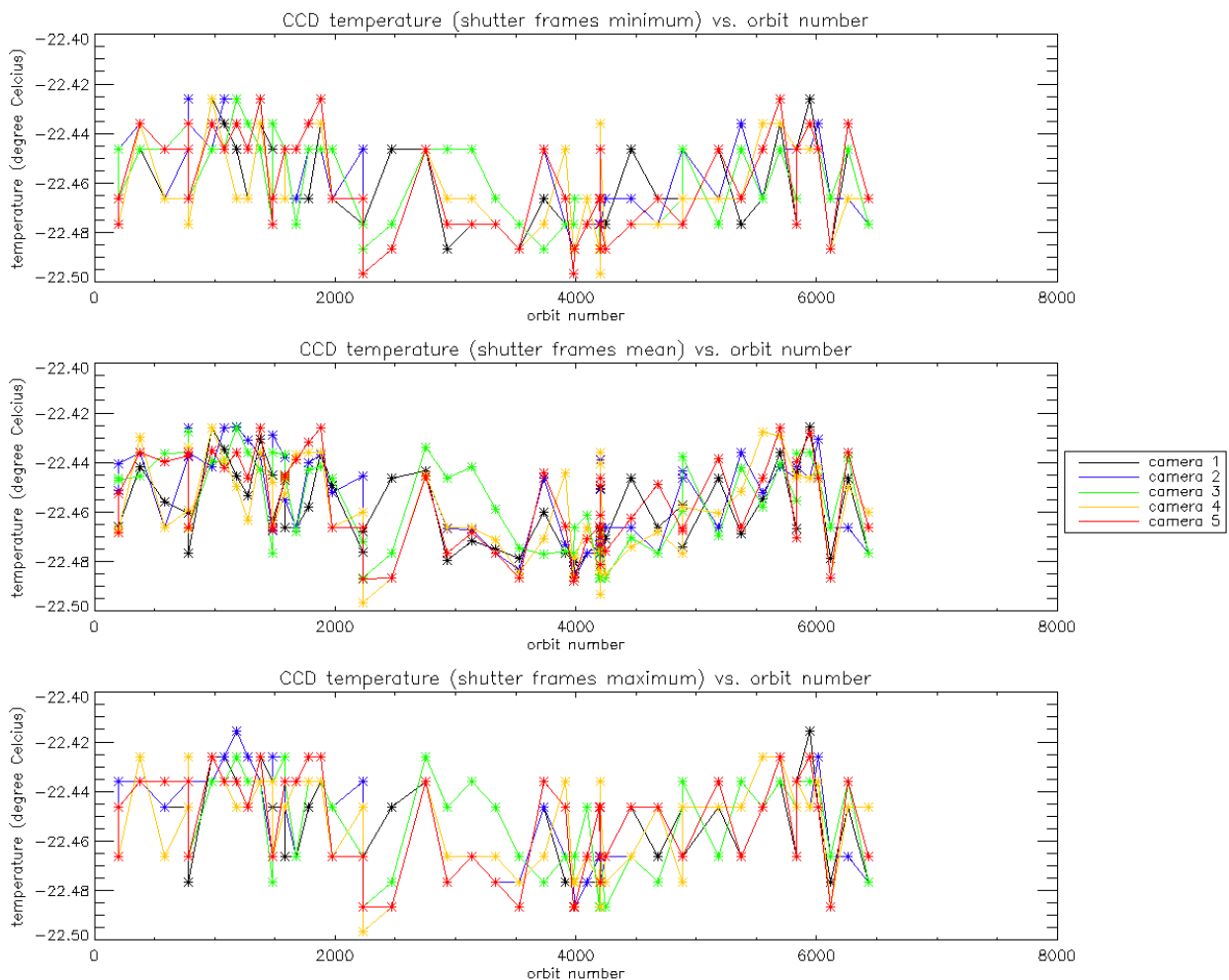


**Figure 1: long term monitoring of CCD temperatures using minimum value (top), time averaged values (middle), and maximum value (bottom) provided in the annotations of the Radiometric Calibration Level 1 products, for the Shutter frames, all radiometric calibrations so far.**

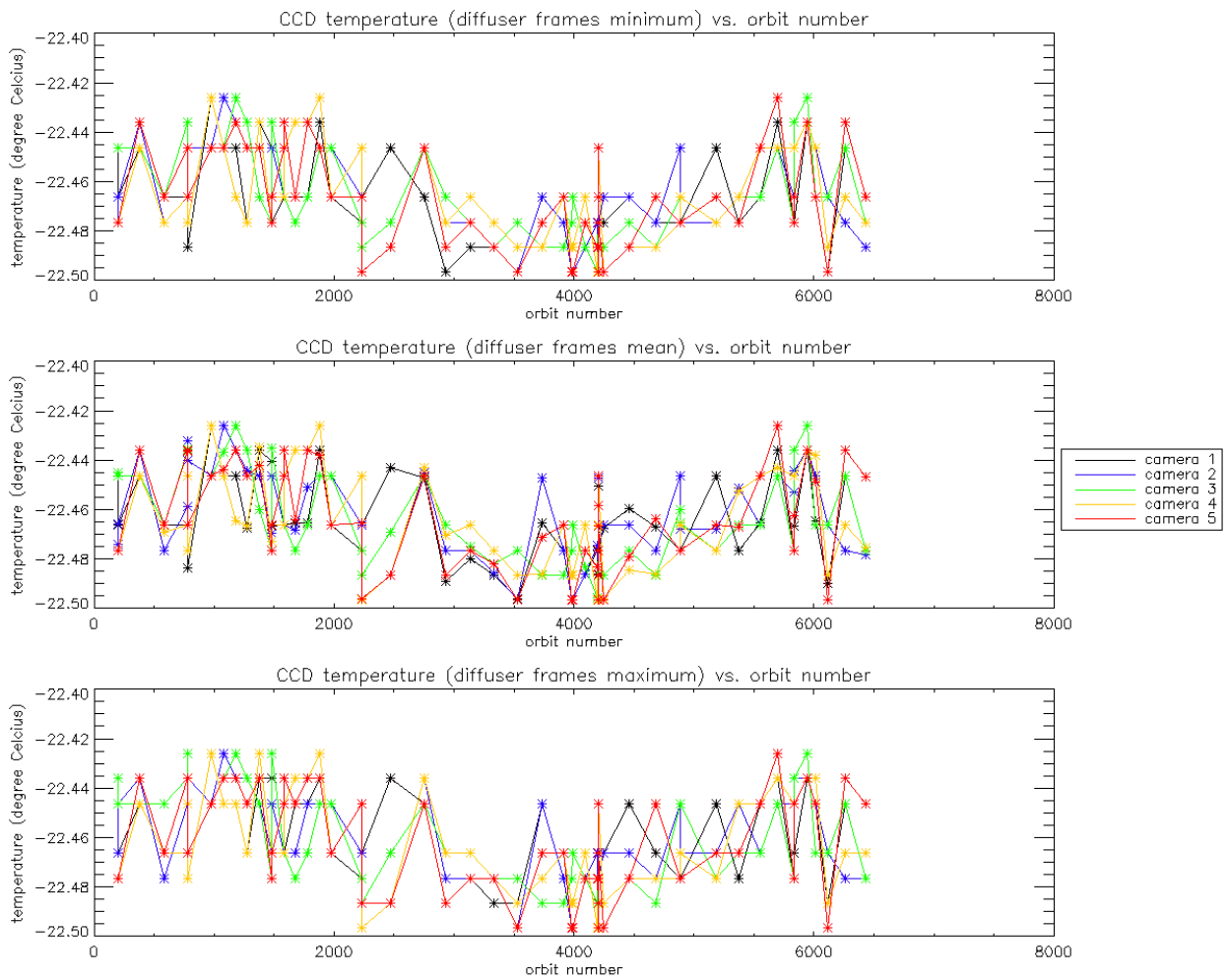


Figure 2: Same as Figure 1 for diffuser frames.

## 1.2 Radiometric Calibration

Two OLCI Radiometric Calibration Sequence have been acquired during Cycle 017:

- ❖ S01 sequence on 30/04/2017 20:50 to 20:52 (absolute orbit 6261)
- ❖ S01 sequence on 12/05/2017 13:54 to 13:56 (absolute orbit 6428)

The acquired Sun azimuth angles are presented on below, on top of the nominal values without Yaw Manoeuvre (i.e. with nominal Yaw Steering control of the satellite).

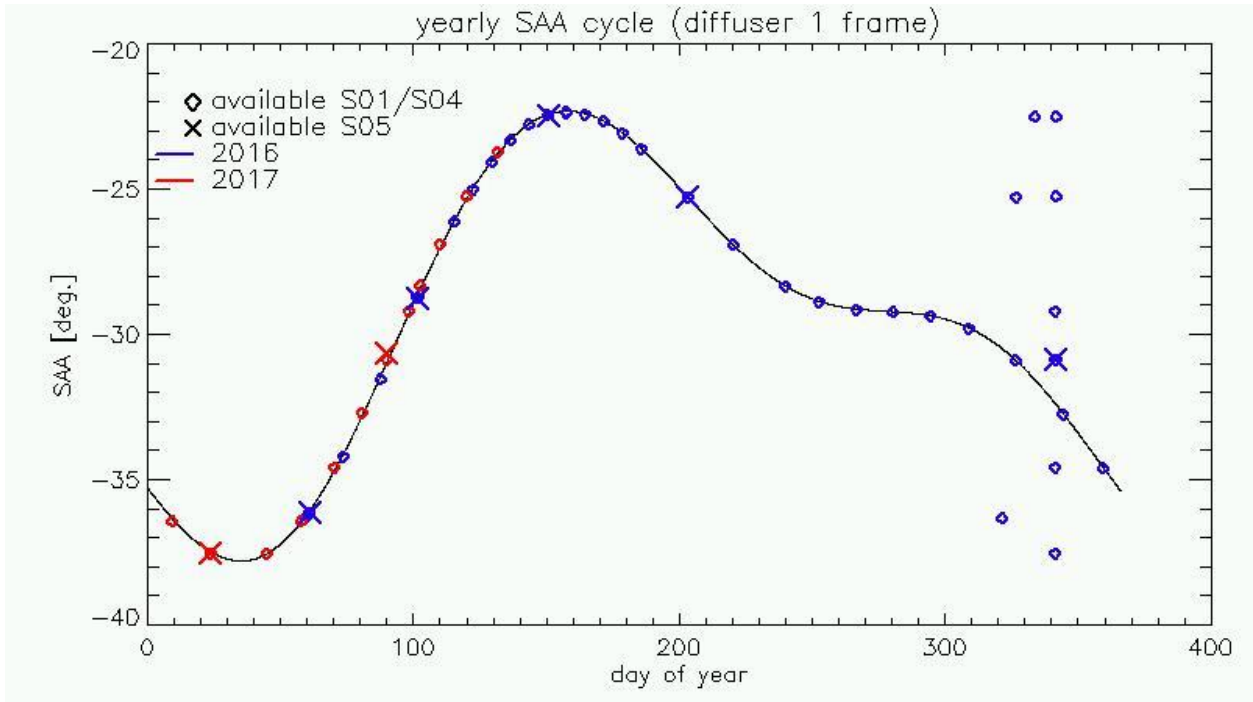


Figure 3: Sun azimuth angles during acquired Radiometric Calibrations (diffuser frame) on top of nominal yearly cycle (black curve). Diffuser 1 with diamonds, diffuser 2 with crosses, 2016 acquisitions in blue, 2017 in red.

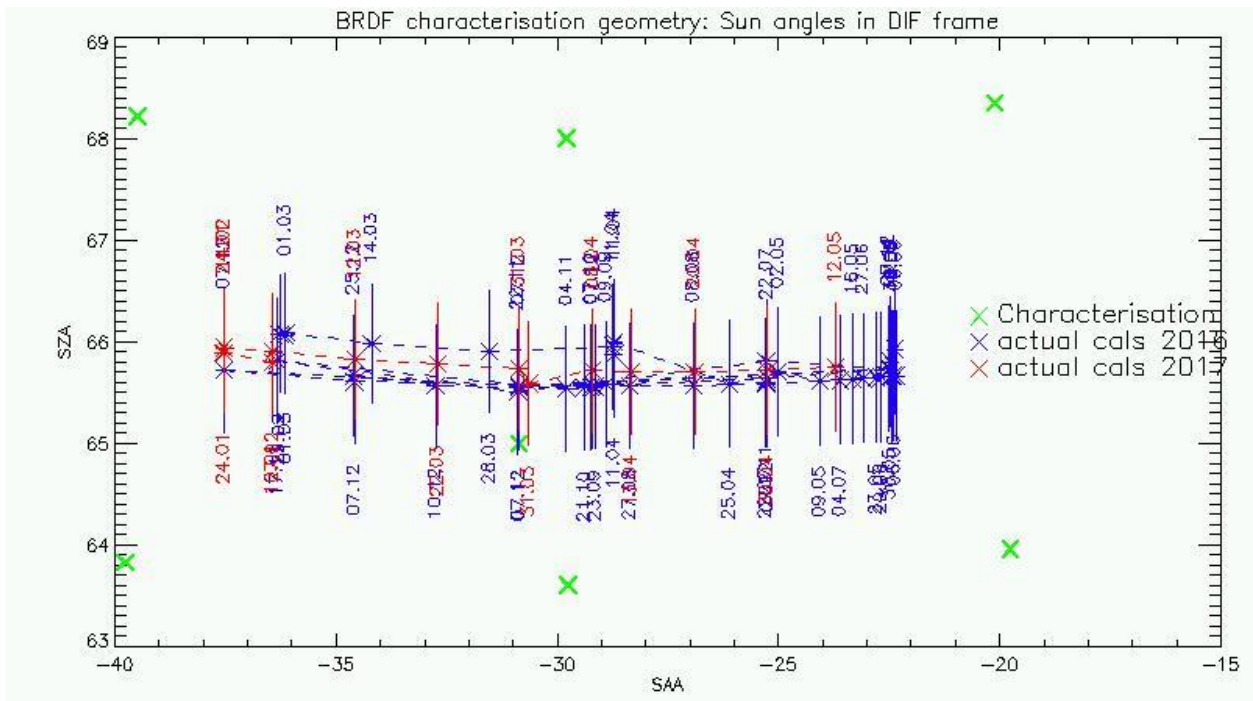


Figure 4: Sun geometry during radiometric Calibrations on top of characterization ones (diffuser frame)

This section presents the overall monitoring of the parameters derived from radiometric calibration data and highlights, if present, specificity of current cycle data.



### 1.2.1 Dark Offsets [OLCI-L1B-CV-230]

#### Dark offsets

Dark offsets are continuously affected by the global offset induced by the Periodic Noise on the OLC convergence. Current Cycle calibrations (orbits 4685, 4887 & 4888) are affected the same way as others. The amplitude of the shift varies with band and camera from virtually nothing (e.g. camera 2, band 0a1) to up to 5 counts (0a21, camera 3). The Periodic Noise itself comes on top of the global shift with its known signature: high frequency oscillations with a rapid damp. This effect remains more or less stable with time in terms of amplitude, frequency and decay length, but its phase varies with time, introducing the global offset mentioned above.

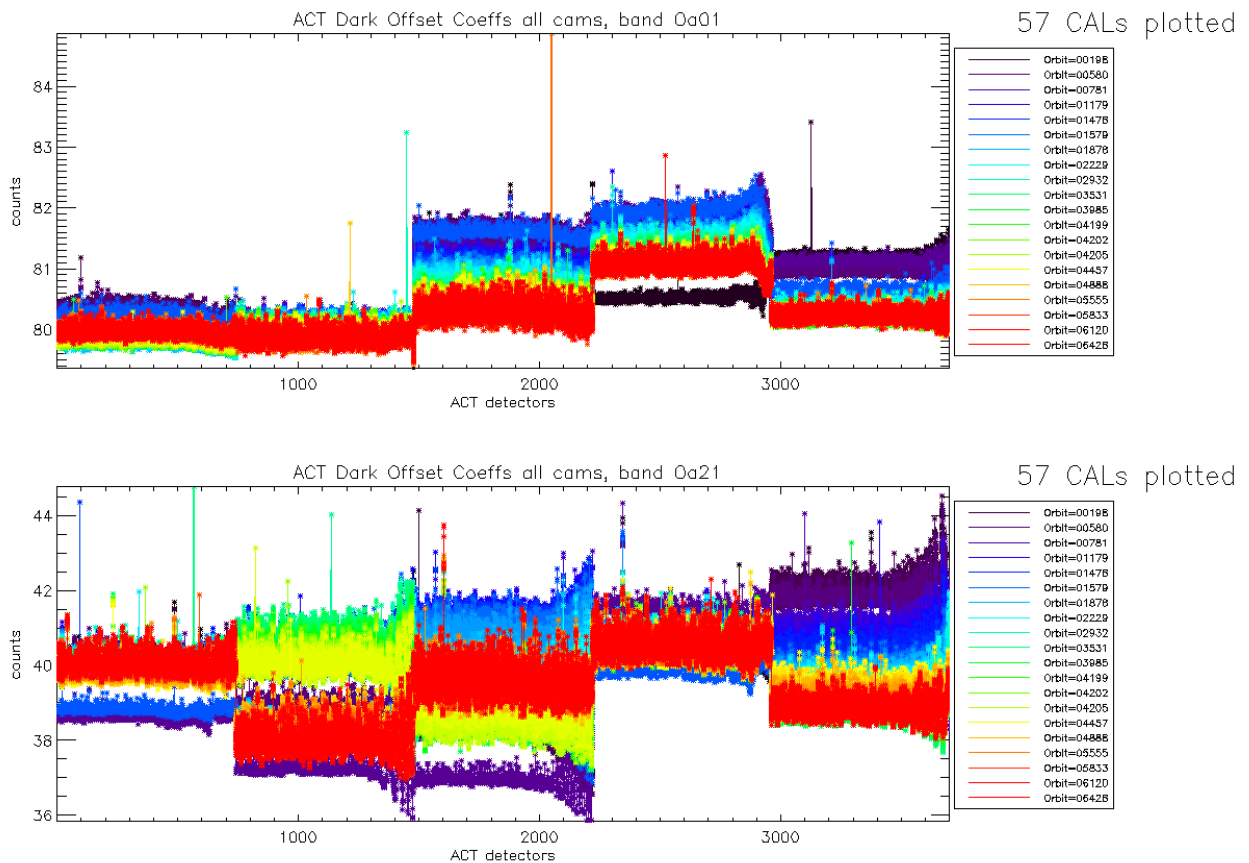
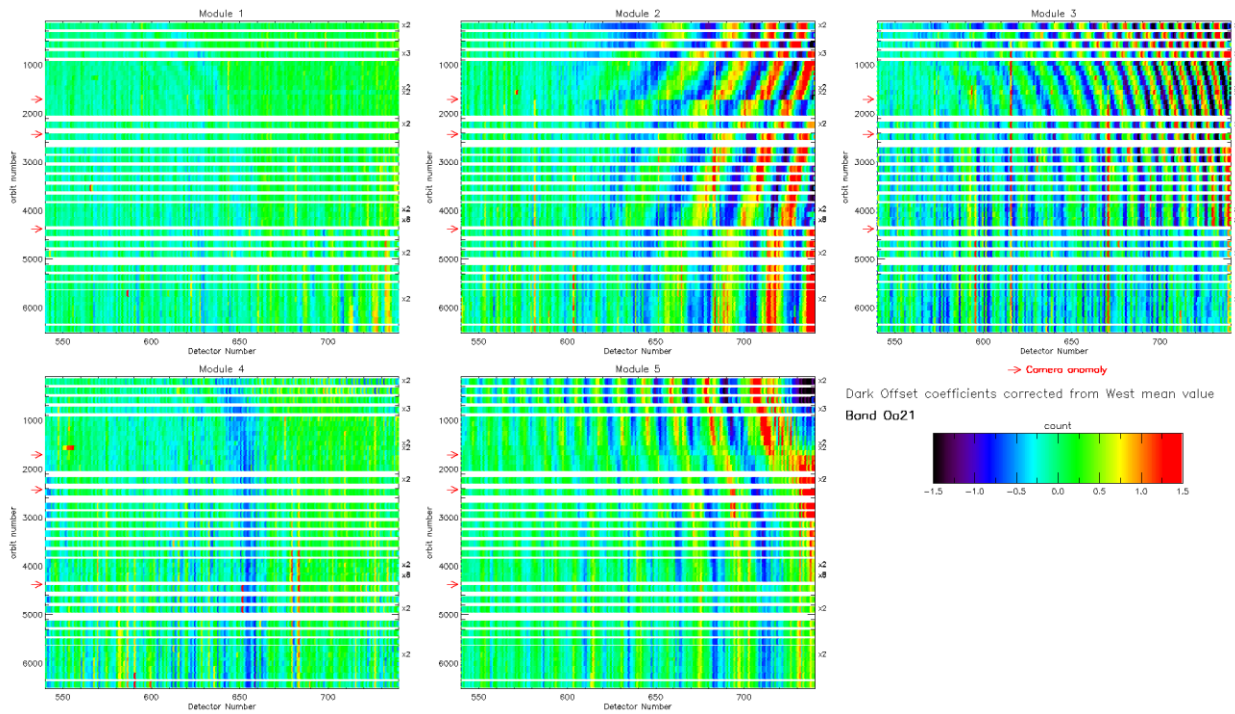


Figure 5: Dark Offset for band Oa1 (top) and Oa21 (bottom), all radiometric calibrations so far except the first one (orbit 183) for which the instrument was not thermally stable yet.



**Figure 6: map of periodic noise for the 5 cameras, for band Oa21. X-axis is detector number (East part, from 540 to 740, where the periodic noise occurs), Y-axis is the orbit number. The counts have been corrected from the west detectors mean value (not affected by periodic noise). Periodic noise amplitude is high in camera 2, 3 and 4. It is lower in camera 4 and small in camera 1.**

Looking at Figure 5 shows no significant evolution of this parameter during the current cycle. Figure 6 shows that since the last sudden PN change (phase and amplitude) caused by the camera-2 anomaly at orbit 4364 (18 December 2016), PN is nearly stabilized again. (See in particular cameras 2, 3 & 5).

### Dark Currents

Dark Currents are not affected by the global offset of the Dark Offsets, thanks to the clamping to the average blind pixels value. However, the oscillations of Periodic Noise remain visible. There is no significant evolution of this parameter during the current cycle.

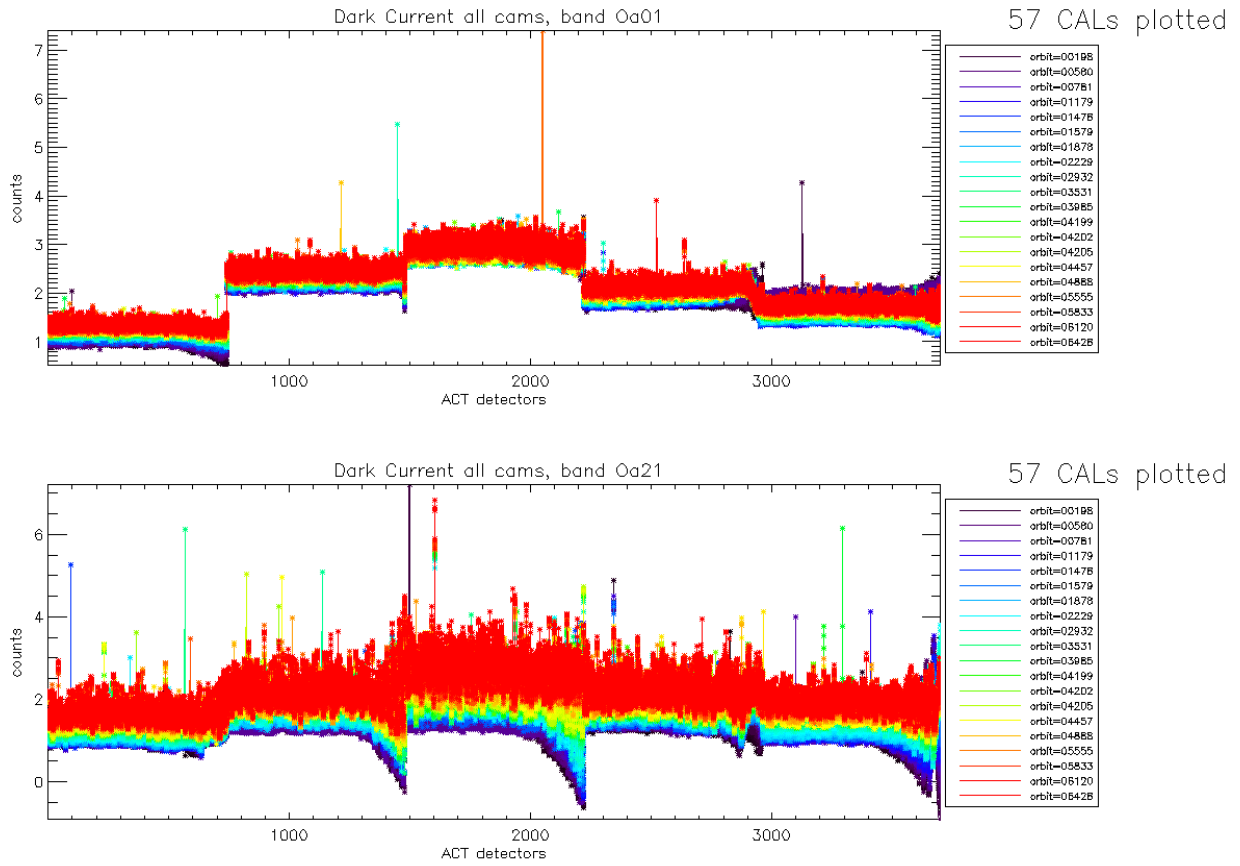


**Figure 7: Dark Current for band Oa1 (top) and Oa21 (bottom), all radiometric calibrations so far except the first one (orbit 183) for which the instrument was not thermally stable yet.**

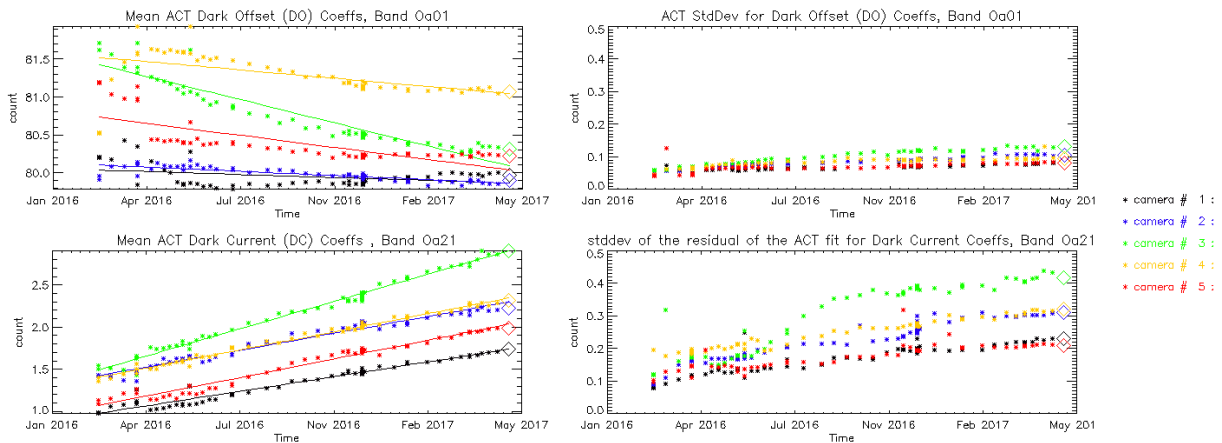


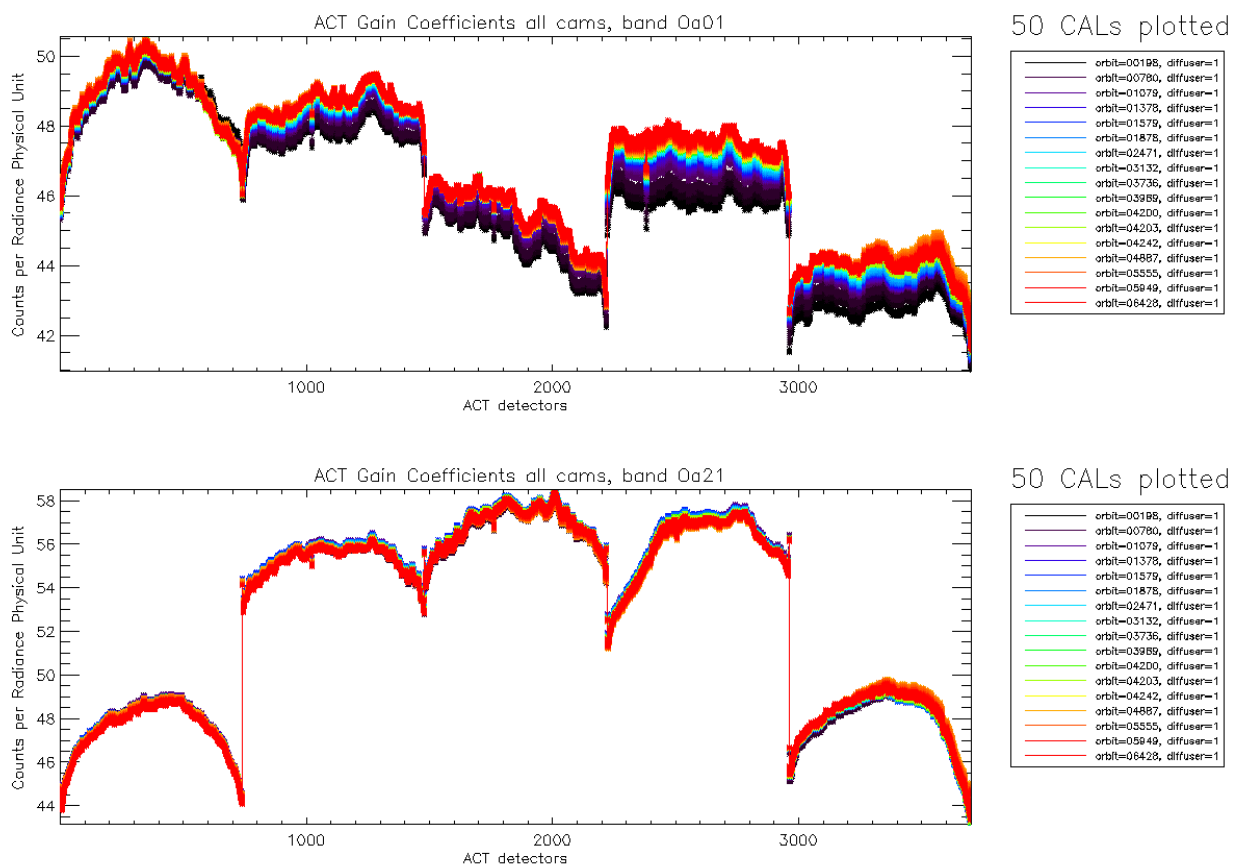
**Figure 8: left column: ACT mean on 400 first detectors of Dark Current coefficients for spectral band Oa01 (top) and Oa21 (bottom). Right column: same as left column but for Standard deviation instead of mean. We see an increase of the DC level as a function of time especially for band Oa21. A possible explanation could be the increase of the number of hot pixels which is more important in Oa21 because this band is made of more CCD lines than band Oa01 and thus receives more cosmic rays impacts. It is known that cosmic rays degrade the structure of the CCD, generating more and more hot pixels at long term scales.**

## 1.2.2 Instrument response and degradation modelling [OLCI-L1B-CV-250]

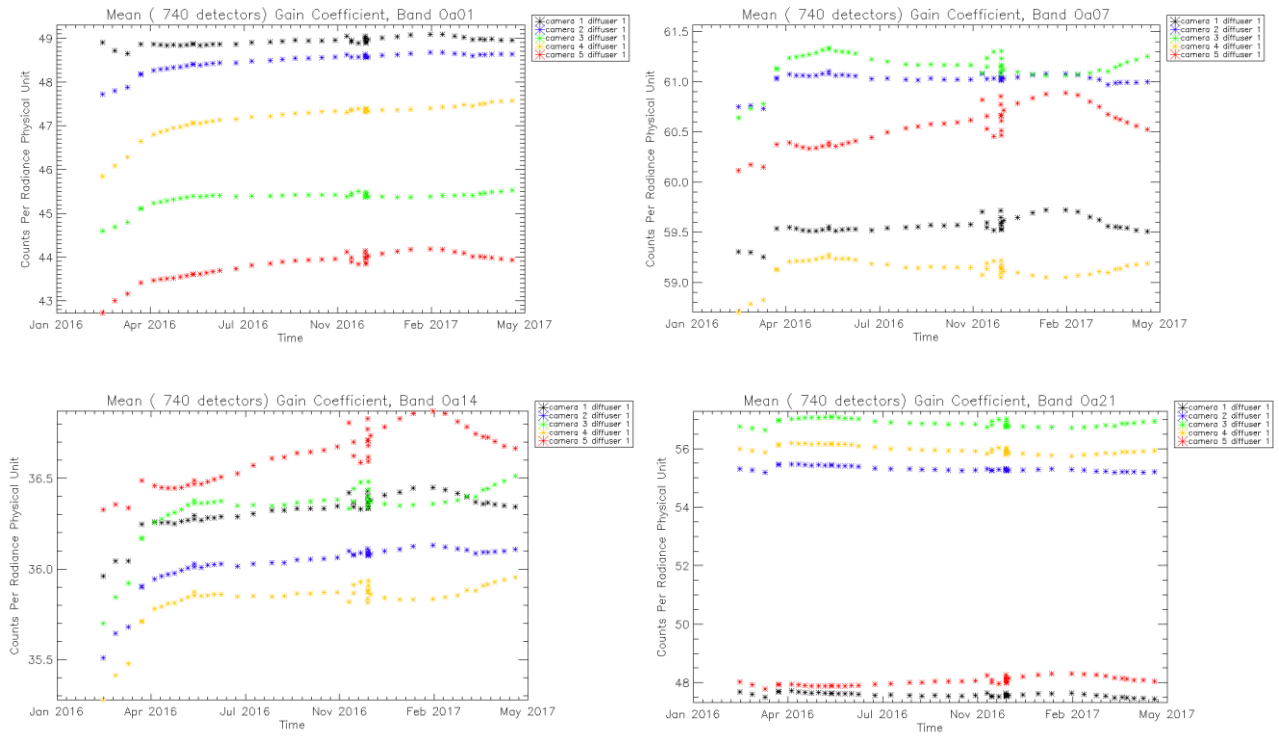
### 1.2.2.1 Instrument response monitoring

Figure 9 below shows the gain coefficients of every pixel for two OLCI channels, Oa1 (400 nm) and Oa21 (1020 nm), highlighting the significant evolution of the instrument response since early mission.

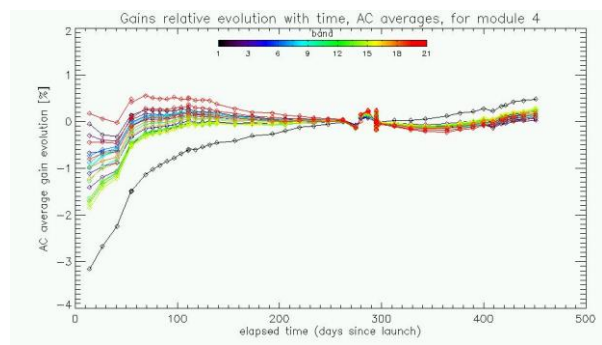
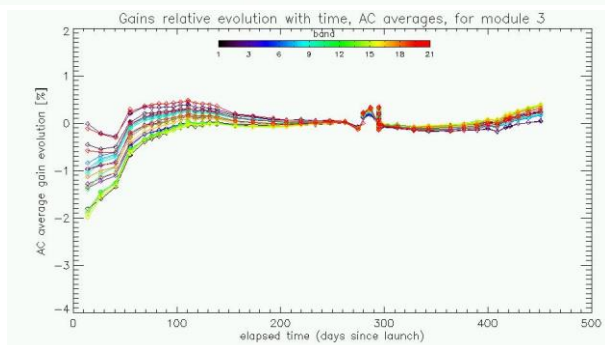
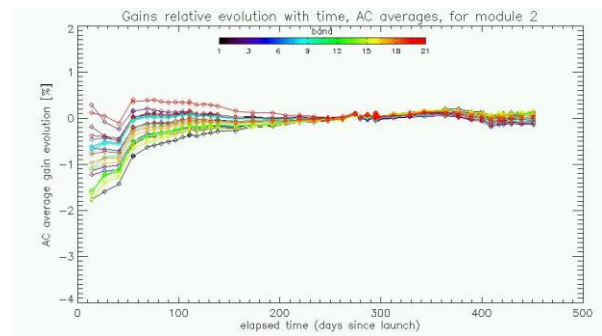
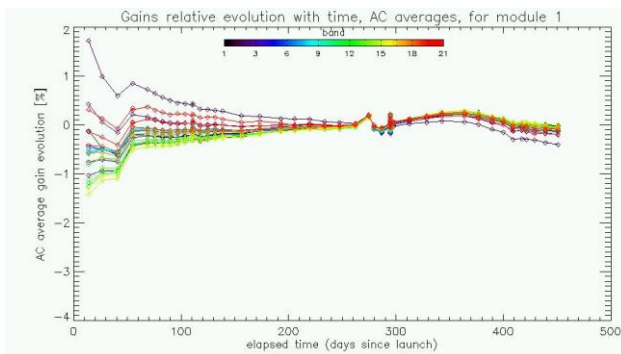
Figure 10 on the other hand displays the time evolution of the cross-track averaged gain, for each module, as a function of time. It shows that if a significant evolution occurred during the early mission, the trends tend to stabilize, with a noticeable exception during the Yaw Manoeuvres (YM) and after, pointing at the dependency of the BRDF model performance with Sun azimuth (on purpose large variations during YM, due to the shape of the seasonal cycle since then). In particular all calibrations between beginning of August and early December (YM) provide very stable results, within 0.5% for all bands. This is further illustrated on Figure 11. The latter shows that radiometric gains are becoming very stable over this period but starts to vary again when the first Yaw Manoeuvre tests come into play, illustrating the influence of geometry. Calibrations acquired during the current cycle, acquired with nominal Yaw Steering, confirm these findings.



**Figure 9: Gain Coefficients for band Oa1 (top) and Oa21 (bottom), all diffuser 1 radiometric calibrations so far except the first one (orbit 183) for which the instrument was not thermally stable yet.**



**Figure 10: time evolution of the camera-averaged Absolute gain coefficients for bands Oa1, Oa7, Oa14 and Oa21 (from left to right and top to bottom).**



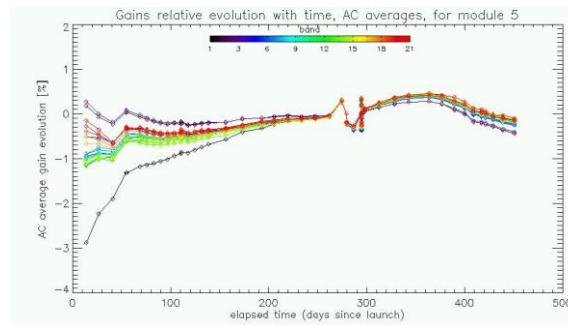


**Figure 11: camera averaged gain relative evolution with respect to “best geometry” calibration (22/11), as a function of elapsed time since first calibration acquired after the fix of the Start Trackers issue; one curve for each band (see colour code on plots), one plot for each module.**

Figure 12 further explore the geometry dependency at short and large time distances, selecting as reference the geometry that best match that of the BRDF modelling lowest residuals. Last two S01 calibrations (current cycle) as well past ones with about the opposite SAA differences are compared against the chosen reference (22/11). The impact is clearly seen, with a significant SAA dependent evolution that can be seen globally as a “white” curvature of the AC profile, increasing with azimuth difference, and with opposite curvature according to the sign of the azimuth difference. On the other hand, the instrument evolution is also clearly visible comparing ratios at symmetrical SAA differences but time lags with opposite signs (top-left with bottom right, top right with bottom left and to a lesser extent top right with centre left panes).

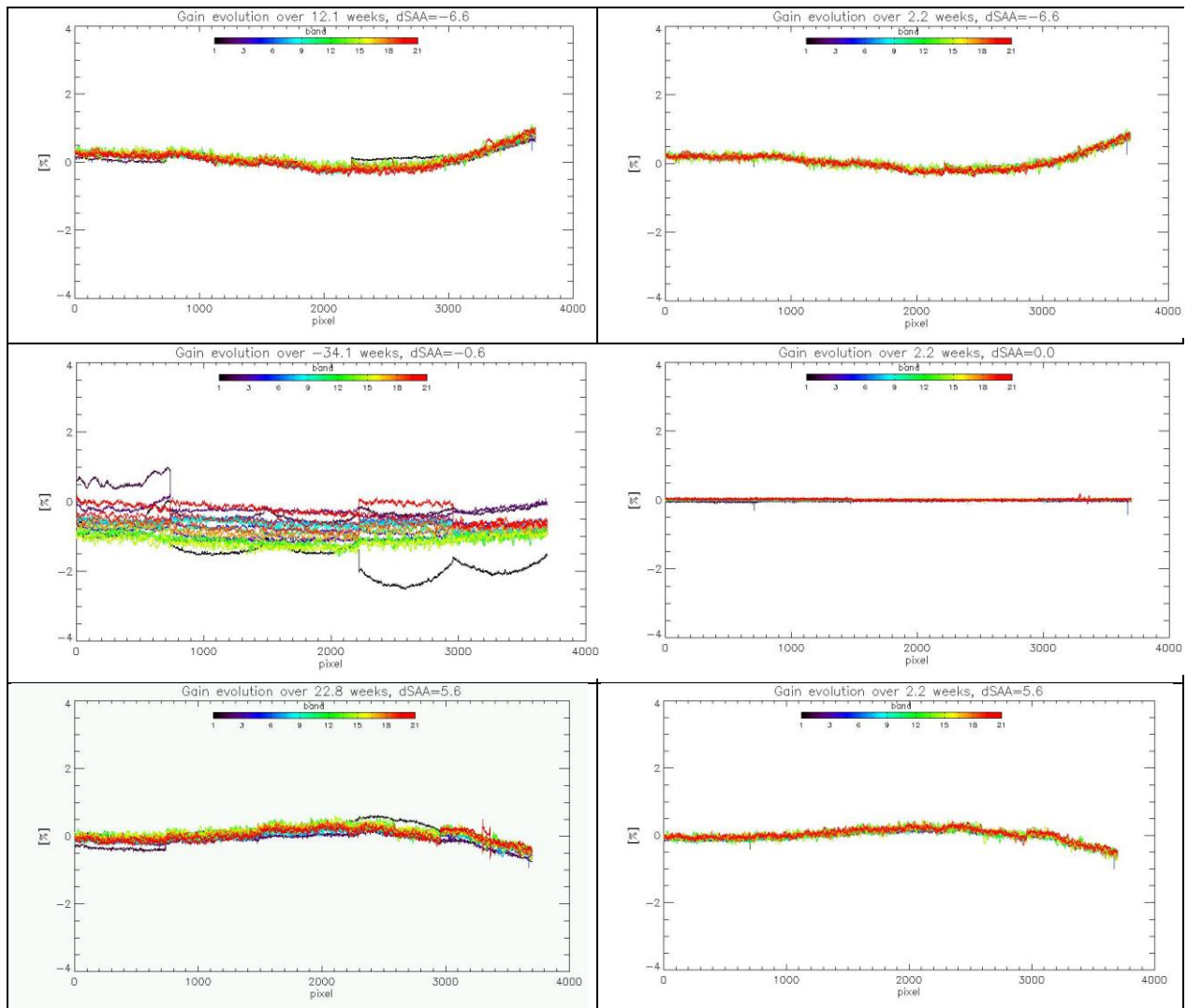


**Figure 12: Across-track profiles of Gains relative evolution with respect to “best geometry” calibration over a relatively large time distance (from -34 to +12 weeks) and for varying geometries, more or less symmetrical with respect to reference one: on the right column time distance remains almost constant around 2 weeks, as calibrations compared to reference are selected within the Yaw Manoeuvres with SAA differences of -6.6, 0 and 5.6 degrees from top to bottom, the left column shows the comparisons at equal or close  $\delta$ SAA than right column, but as large as possible time distance.(from top to bottom time differences are respectively +12,-34 and +22.8 weeks). Influence of geometry and time are both clearly visible and can be distinguished from each other.**

In order to get rid of the white variability (not spectrally dependant) caused by the BRDF model, all bands are normalized by band Oa18. Oa18 was chosen because NIR degrades slowest and because Oa20 and Oa21 are subject to Periodic Noise, e- leaks, etc ... Results are presented Figure 13.

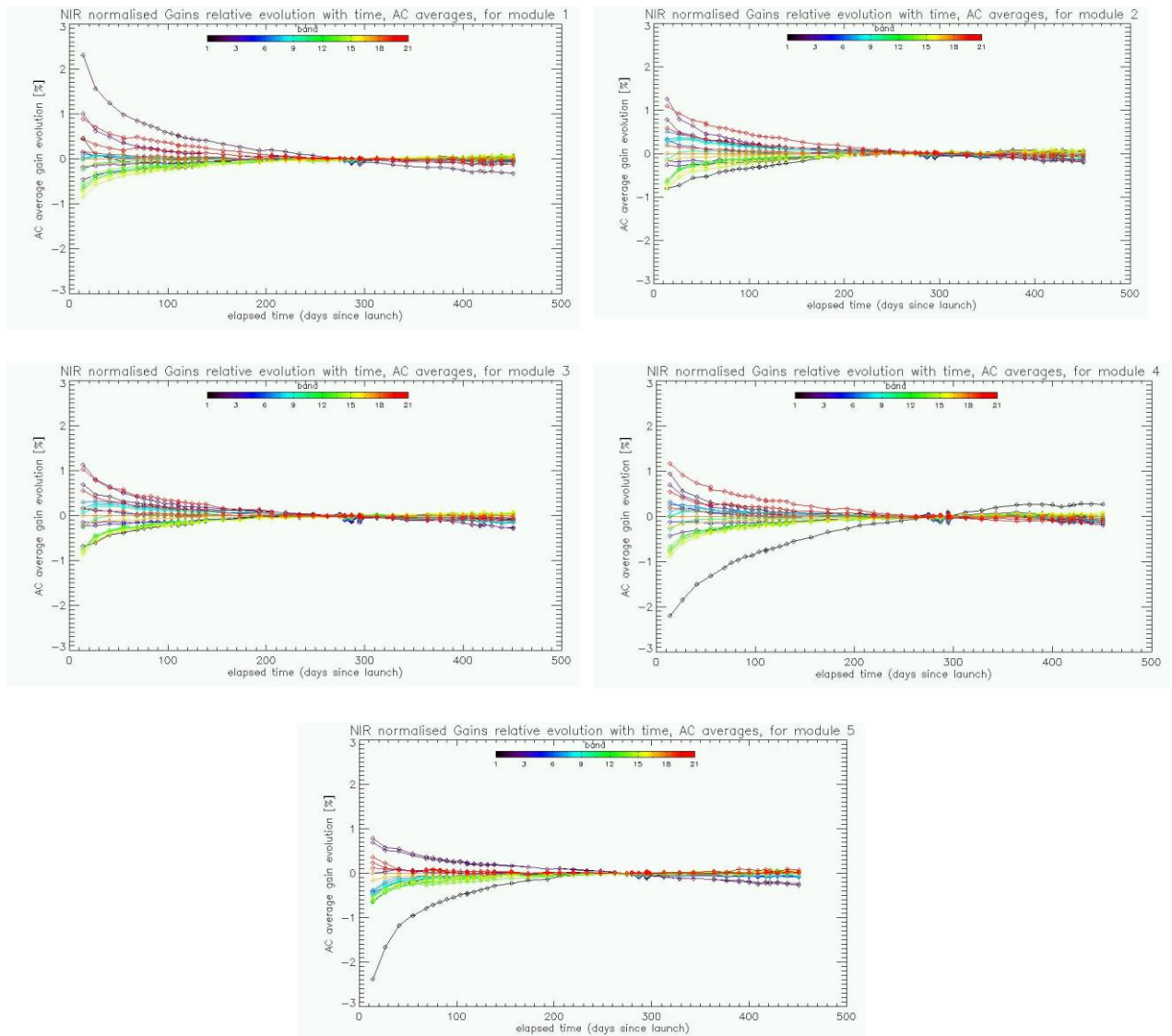


Figure 13: same as Figure 11 after normalization by band Oa18.

In Figure 13, we see that the ugly oscillations of Figure 11 have disappeared. However it is still surprising that some bands show an increase of sensitivity with time, while a decrease is expected since we are monitoring a 'degradation' of the instrument. Using the diffuser 2 results, we can say that this sensitivity increase cannot be explained by the ageing of diffuser 1. Moreover, we have checked that the spectral assignment drift cannot explain either this increase of sensitivity. Figure 14, compared to Figure 12, allows verifying the performance of the BRDF error correction on AC profiles.

Thus there is still something that remains unexplained concerning the evolution of the sensitivity of the instrument. Investigations are on-going.

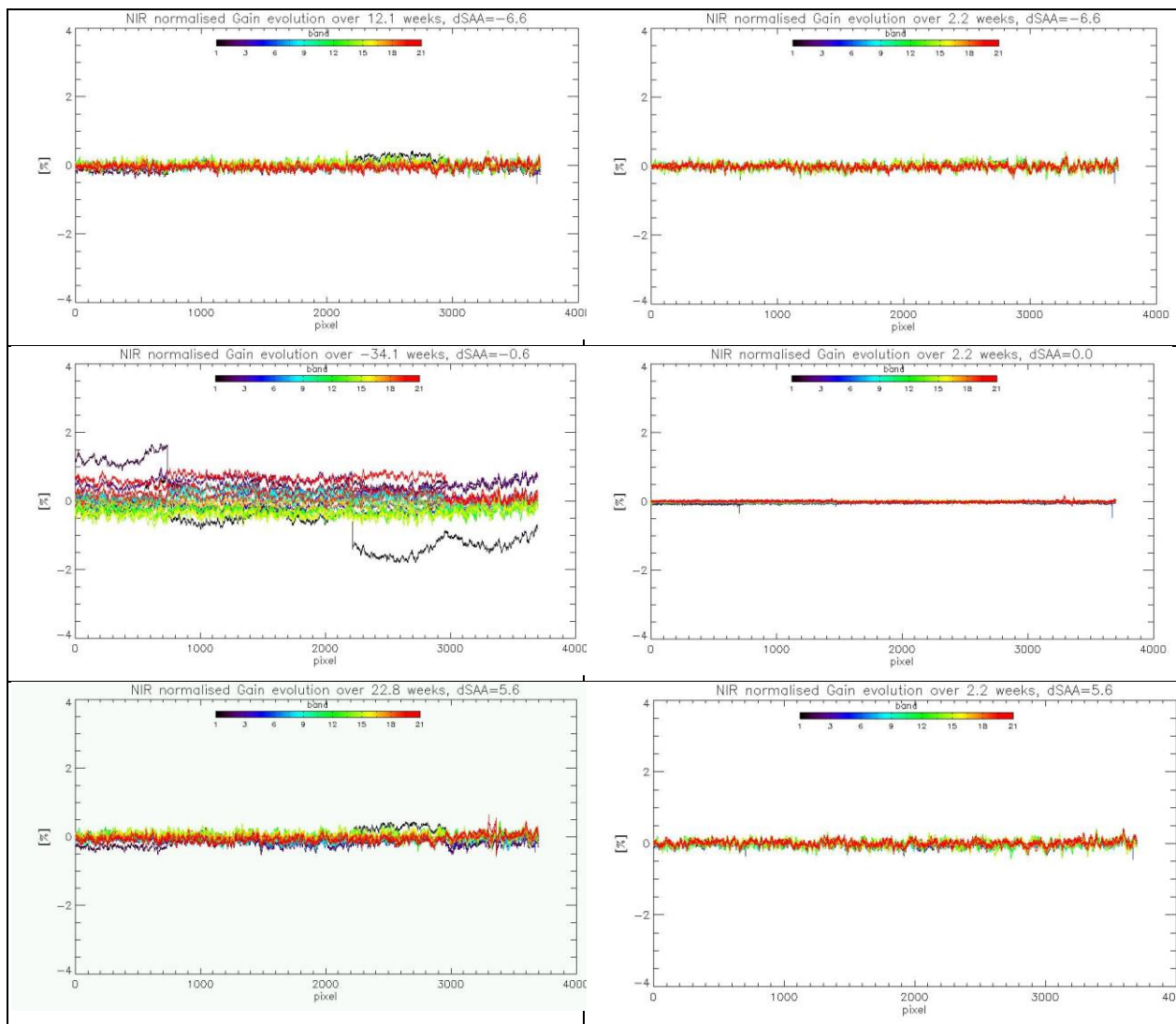
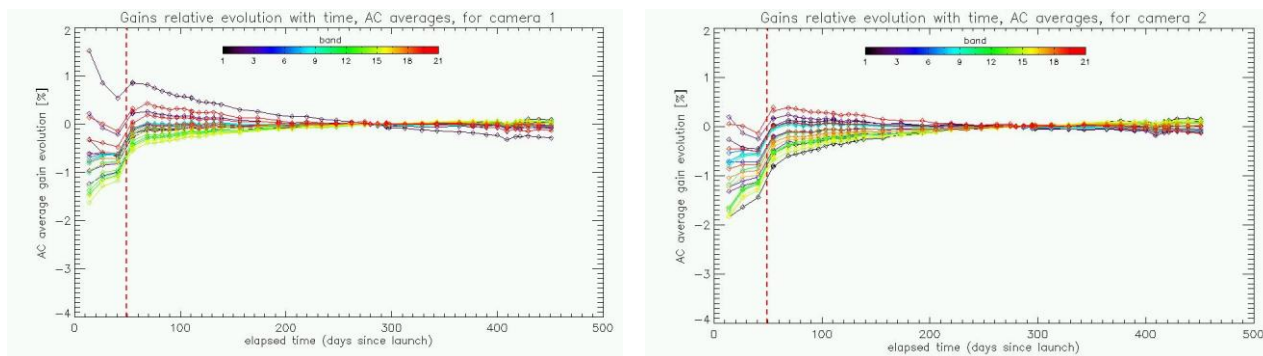
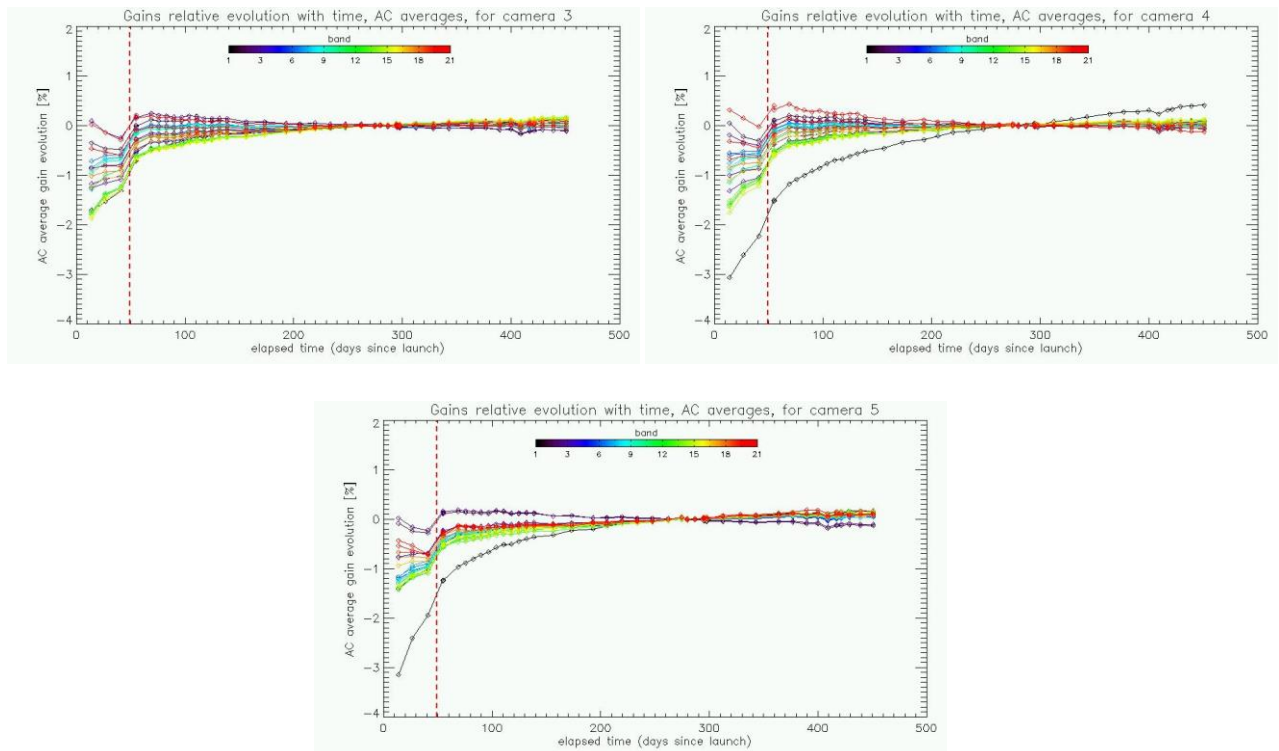


Figure 14: same as Figure 12 after normalization by band Oa18.

In Figure 15, we plot the gain evolution when using the updated diffuser BRDF model (derived thanks to the Yaw Manoeuvre data of 7 DEC 2016) instead of the pre-flight BRDF model, affected by significant dependency with Sunb geometry.





**Figure 15: same as Figure 11 but using the updated BRDF model. The data have NOT been normalized by band Oa18. The star tracker anomaly fix is represented by a vertical red dashed line.**

Comparing Figure 15 (new BRDF model, no normalization) and Figure 13 (old BRDF model, normalization by NIR band Oa18), we see that the radiometric evolution derived using both methods show fairly comparable general trend, in particular when excluding the Star Tracker anomaly period. The behaviour over the first two months of mission, affected by the Star Tracker anomaly, is really different: The normalization to NIR completely hides the BRDF error due to the wrong platform attitude while it becomes obvious using the updated BRDF model without normalization.

### 1.2.2.2 Instrument evolution modelling

Thanks to the work done on the Yaw Manoeuvres Calibration acquisitions (see section 1.2.5) an upgraded diffuser BRDF model has been derived, allowing to get rid of the operational model dependency with Sun azimuth discussed above. This in turn allowed, first to justify a posteriori the NIR normalization approach, as the evolution of band Oa18 – assumed negligible in the normalization process – could be assessed independently as relatively small (<0.2%), but overall to build a global gain database corrected for BRDF error residuals. This database was used as the basis for the derivation of a long-term radiometric drift model.

This required a number of adaptations of the dedicated software for several reasons:

- 1) The upgraded BRDF model is not implemented in the Calibration processing software (IPF OL1-RC), thus the derived gains have to be corrected for BRDF in a post-processing step, on the

(justified) assumption that the BRDF changes have a second order impact on the stray-light computation.

- 2) The observed instrument evolution does not follow the expected behaviour: a slow and smooth instrument sensitivity decrease, but on the contrary can show increase as well (see Figure 16))
- 3) The time period is not long enough to correctly model the evolution for cameras/channels for which it is very small: in this case the signal to noise ratio (e. g. due to diffuser speckle) is not high enough and the fit parameters that provide the best match are not physical. As a consequence, it may happen that, despite the model matches very well to the data, its use in extrapolation generates huge drifts that are very unlikely to occur. A post-processing is thus necessary to identify and update those cases.

The model has been derived from the dataset ranging from 26/04/2016 to 12/03/2017, so that the validation dataset now includes 7 calibrations over 3 months for performance estimation, including the 2 calibrations acquired during current cycle.

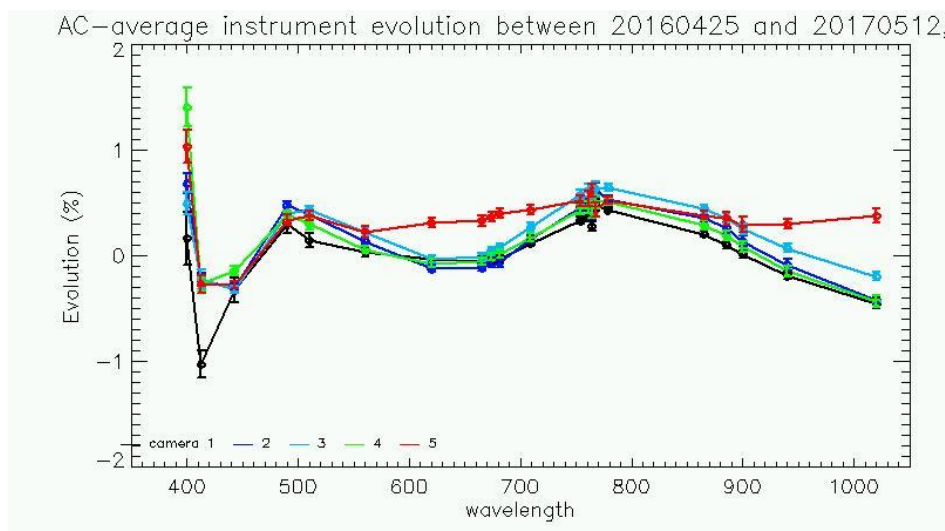


**Figure 16: Camera-averaged instrument evolution since channel programming change (25/04/2016) and up to most recent calibration (12/05/2017) versus wavelength.**

Once these steps are completed, the model performance over the complete dataset (including 7 calibrations in extrapolation over up to 3 months) is better than 0.2% except at very specific cases: few isolated pixels in about half of the bands, and two specific features in camera 5 for channels Oa8 and Oa21 that cannot be fitted with a bounded exponential model. The overall performance at each orbit is shown on as the average and standard deviation of the model over data ratio as a function of wavelength, for each orbit in order to highlight a possible extrapolation issue. If the figure shows an outlying orbit, it must be stressed that it is NOT the most recent, excluding a systematic drift in extrapolation, as proved by Figure 18.

Finally, Figure 19 to Figure 21 show the detail of the model performance, with across-track plots of the model over data ratios at each orbit, one plot for each channel.

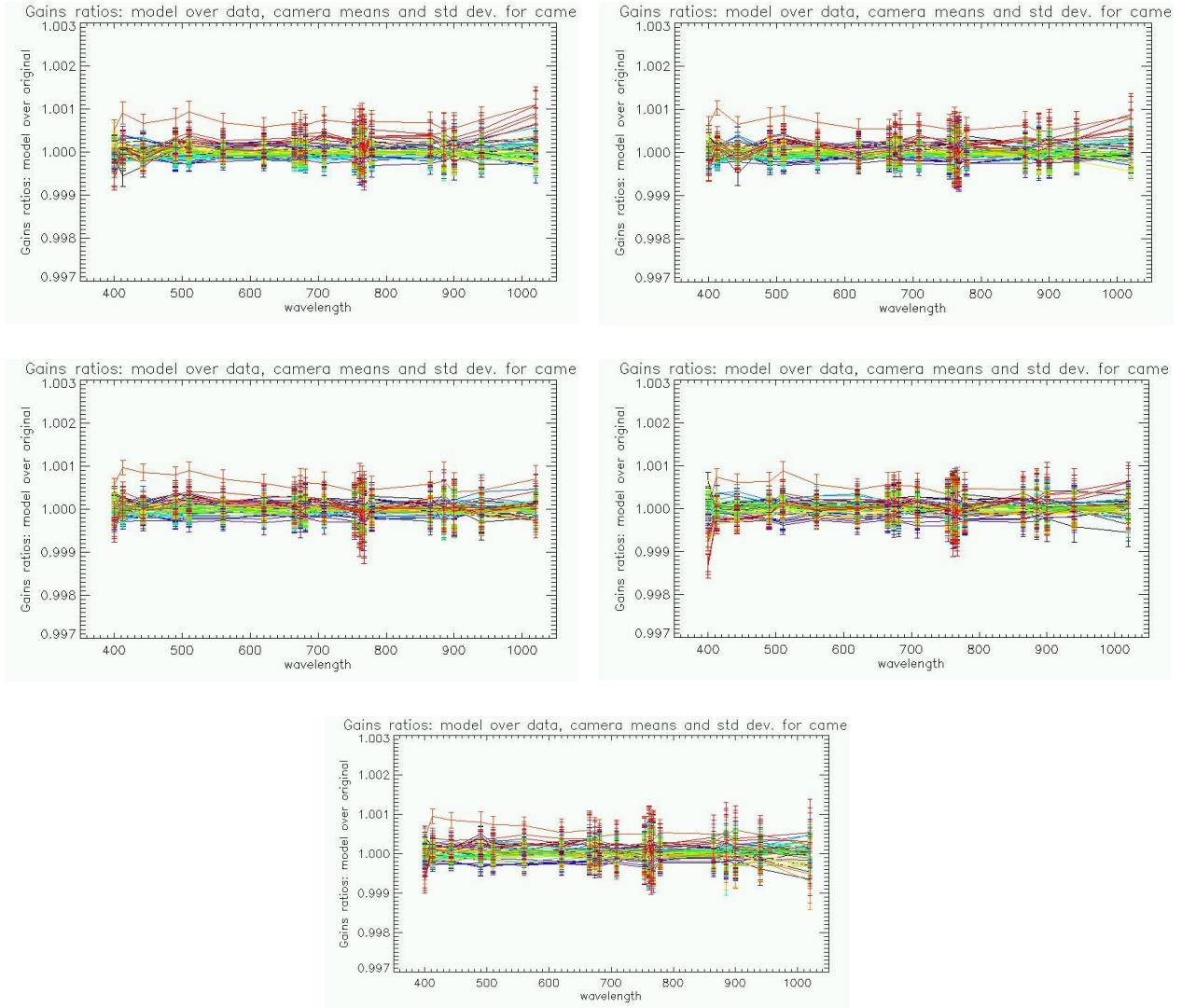


**Figure 17: For the 5 cameras: Evolution model performance, as camera-average and standard deviation of ratio of Model over Data vs. wavelength, for each orbit of the test dataset, including 3 calibration in extrapolation, with a colour code for each calibration from blue (oldest) to red (most recent).**

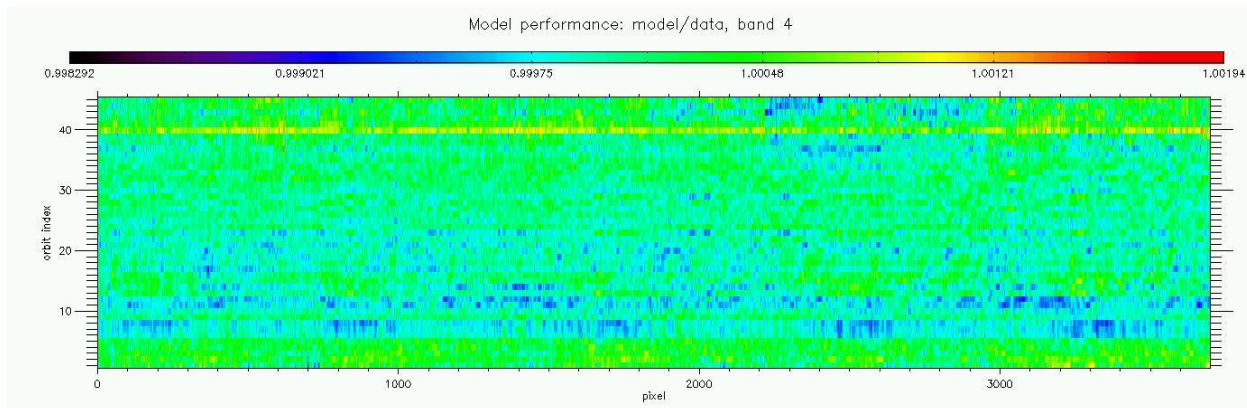


**Figure 18: model performance: ratio of model over data for all pixels (x axis) of all orbits (y axis), for channel Oa4. The outlying orbit #40 is that of 31/03/2017.**

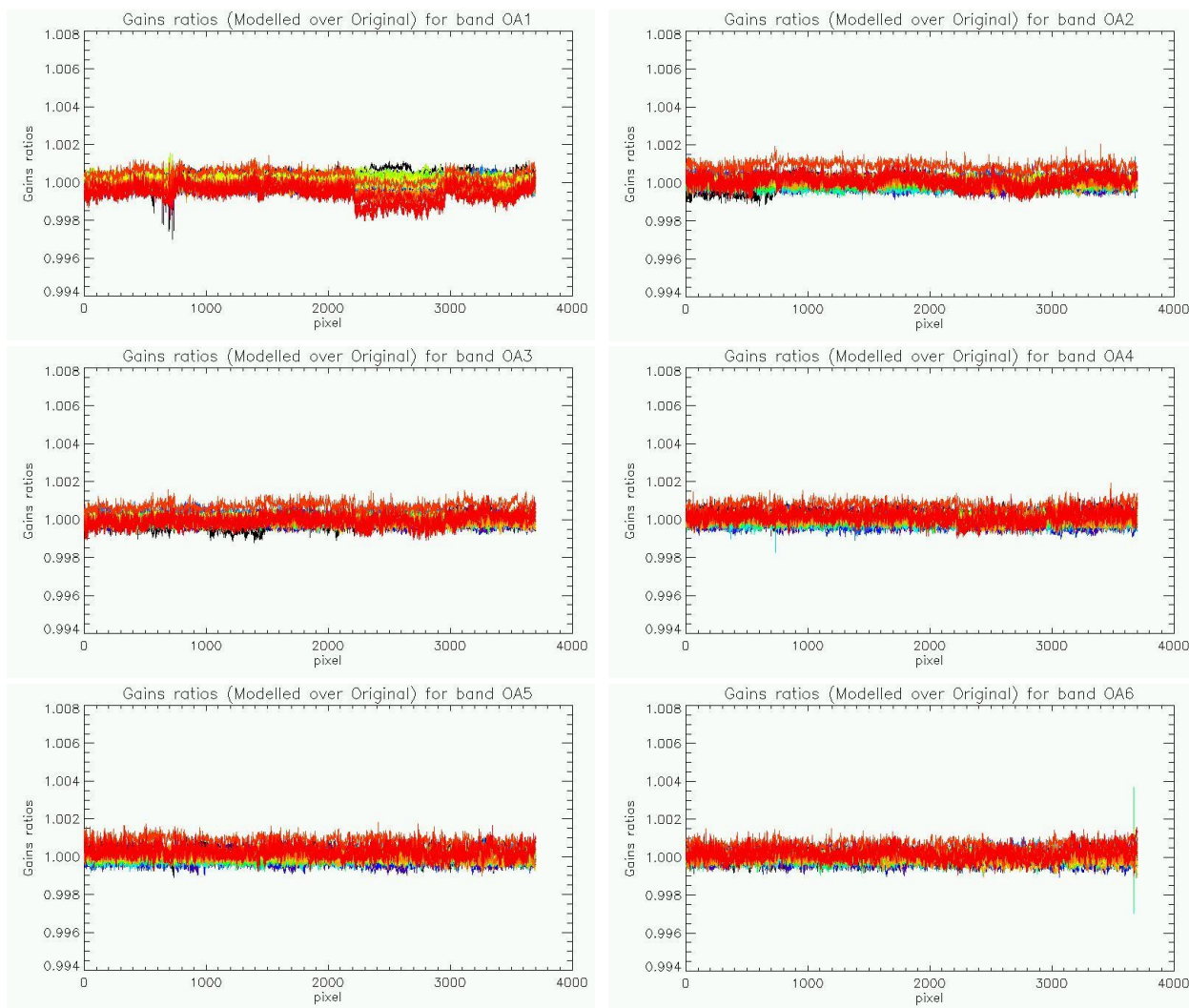


**Figure 19: Evolution model performance, as ratio of Model over Data vs. pixels, all cameras side by side, over the whole current calibration dataset (since instrument programming update), including 7 calibration in extrapolation, channels Oa1 to Oa6.**

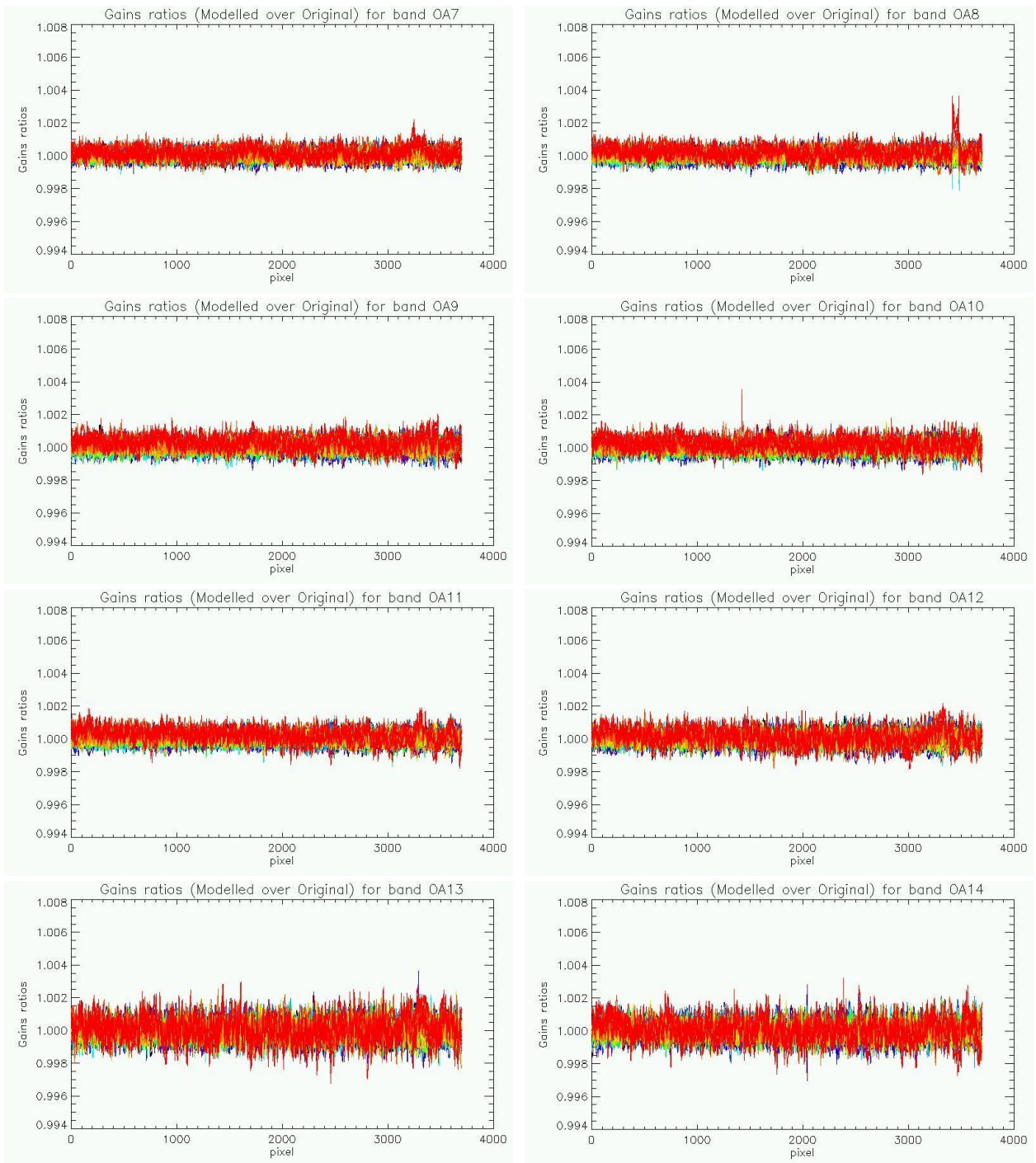


Figure 20: same as Figure 19 for channels Oa7 to Oa14.

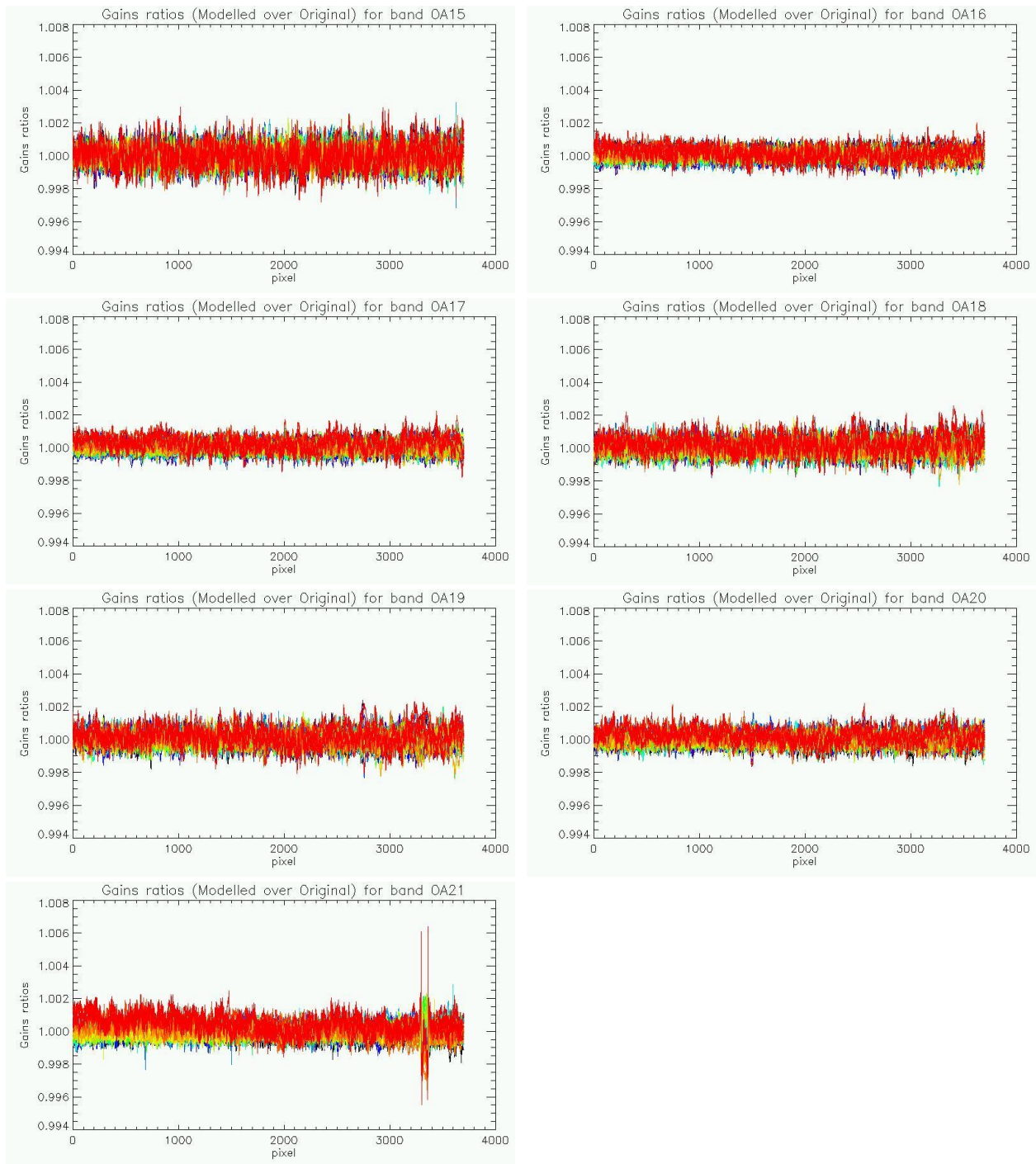


Figure 21: same as Figure 19 for channels Oa15 to Oa21.

### 1.2.3 Ageing of nominal diffuser [OLCI-L1B-CV-240]

There has been no calibration sequence S05 (reference diffuser) acquisition during cycle 017.

Consequently the last updated results are still valid and reported below.

The diffuser 1 Ageing is computed for each 3700 detector and each spectral band by formula:

$$\text{Ageing}(\text{orb}) = G1(\text{orb})/G2(\text{orb}) - G1(\text{orb\_ref})/G2(\text{orb\_ref})$$

Where:

- ❖ G1 is the diffuser 1 (= nominal diffuser) Gain coefficients.
- ❖ G2 is the diffuser 2 (= reference diffuser) Gain coefficients
- ❖ orb\_ref is a reference orbit chosen at the beginning of the mission

Ageing is represented in Figure 22 for band Oa1 and in Figure 23 for band Oa16. The negative shift of the latest sequence (for which a slight increase would be expected instead) is not explained so far and still under investigation. It should be noted that the corresponding orbit of diffuser 1 (nominal) has also been detected as an outlier in the modelling of the radiometric long-term trend (see section 1.2.2.2) with an unexpected excess of brightness.

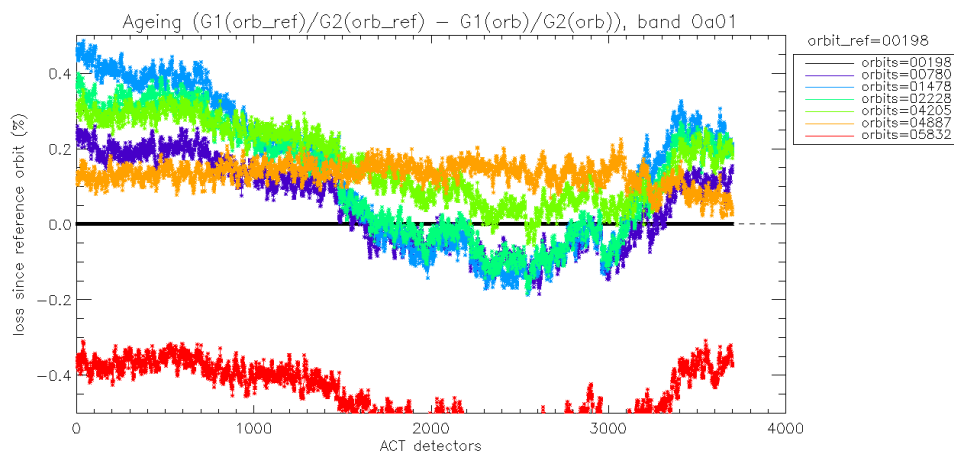


**Figure 22: diffuser 1 ageing for spectral band Oa01. We see strong ACT low frequency structures that are due to residual of BRDF modelling.**

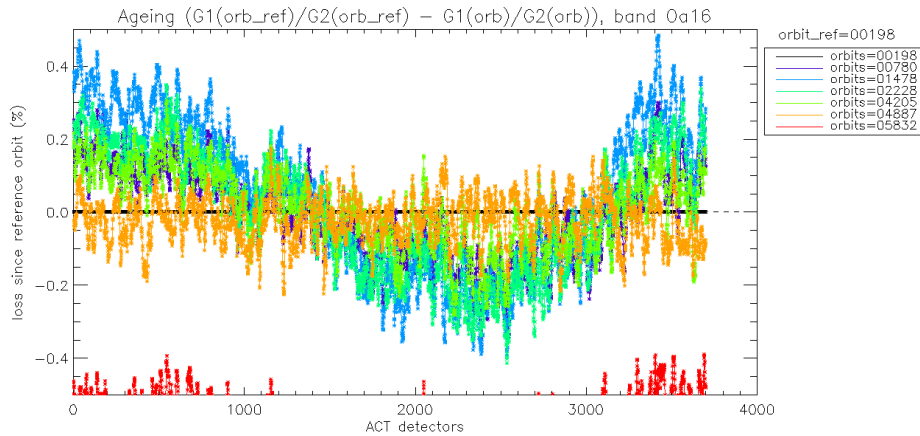


**Figure 23: same as Figure 22 for spectral band Oa16. We use this band in order to normalize other bands and remove the ACT structures due to residual of BRDF modelling. Normalized curve for spectral band Oa01 is presented in Figure 24.**

Figure 22 and Figure 23 show that the Ageing curves are impacted by a strong ACT pattern which is due to residuals of the bad modelling of the diffuser BRDF. This pattern is dependant of the azimuth angle. It is a 'white' pattern which means it is the same for all spectral bands. As such, we can remove this pattern by normalizing the ageing of all bands by the curve of band Oa16 which is expected not to be impacted by ageing because in the red part of the spectrum. We use an ACT smoothed version (window of 100 detectors) of band Oa16 in order to reduce the high frequency noise. Normalized ageing for spectral band Oa01 is represented in Figure 24 where we can see that this band is impacted by ageing of the diffuser.

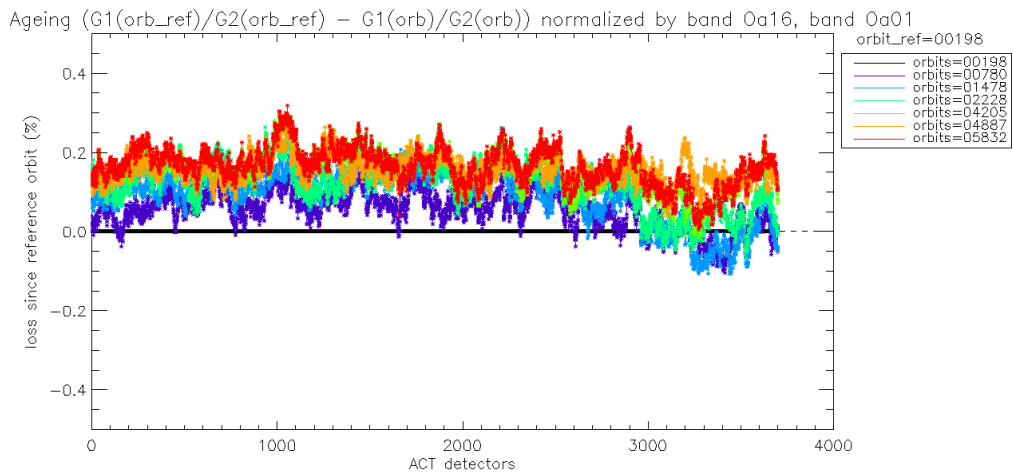


**Figure 24: same as Figure 22 after normalization by band Oa16. Ageing of the diffuser 1 is now visible in the 5 cameras.**



Camera averaged ageing (normalized by band Oa16) as a function of wavelength is represented in Figure 25 where we can see that ageing is stronger in the 'blue' (short wavelengths). Ageing is visible only for the 5 first spectral bands so far in the OLCI mission life.

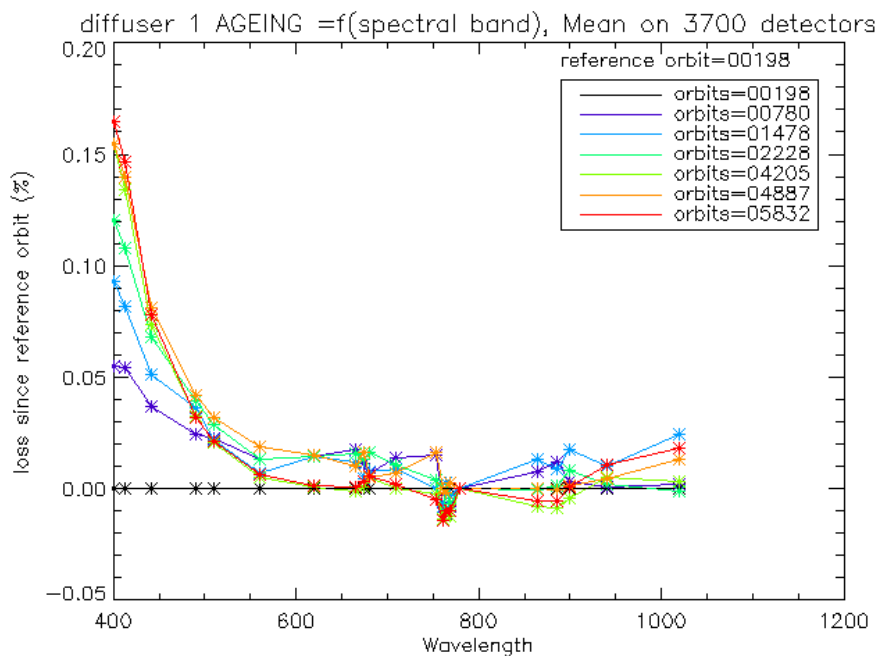


**Figure 25: Diffuser 1 ageing as a function of wavelength (or spectral band). Ageing is visible in spectral band #1 to #5.**

Figure 26 shows the evolution of the 5 camera averaged ageing as a function of time.

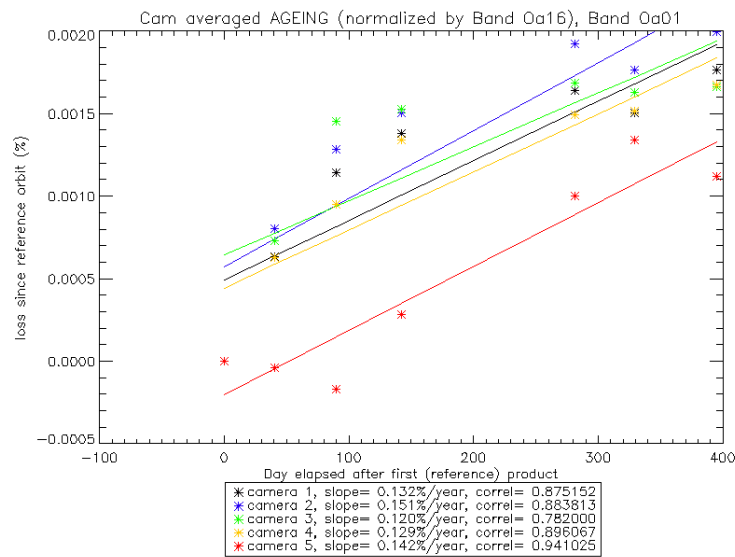


**Figure 26: Camera averaged ageing (normalized by band Oa16) as a function of time. Linear fit for each camera is plotted. The slope (% loss per year) and the correlation coefficient of the linear fits are written in the legend at the bottom.**

#### 1.2.4 Updating of calibration ADF [OLCI-L1B-CV-260]

A number of OL\_1\_CAL\_AX have been generated during cycle 017, to host the recently defined Radiometric Gain model (including long-term drift, see section 1.2.2.2) as well as frequently refreshed Dark Correction LUTs, covering the 25/04/2016 to present period. It includes the following evolution:

1. A common radiometric gain model for all, based on the long-term drift modelling described in section 1.2.2.2, and a reference gain derived from the average of all calibrations within [25/04/2016, 12/03/2017] once corrected for the drift,
2. Frequent update of the Dark Offset and Dark Current LUTs to minimise the impact of Periodic Noise: all calibrations with OCL ON have been selected, except those too close to their immediate predecessor (in practice this eliminates mostly the S05 of ageing sequences, 1 orbit later than S04 or S01). Validity dates have been set starting from the used calibration sequence and ending at next selected one, i.e. without any overlap.

The list of generated ADFs is:

S3A\_OL\_1\_CAL\_AX\_20160425T103700\_20160502T105515\_20170426T171557\_\_\_\_\_MPC\_O\_AL\_R02.SEN3  
 S3A\_OL\_1\_CAL\_AX\_20160502T105515\_20160509T111321\_20170426T171557\_\_\_\_\_MPC\_O\_AL\_R02.SEN3  
 S3A\_OL\_1\_CAL\_AX\_20160509T111321\_20160516T113134\_20170426T171557\_\_\_\_\_MPC\_O\_AL\_R02.SEN3  
 S3A\_OL\_1\_CAL\_AX\_20160516T113134\_20160523T100851\_20170426T171557\_\_\_\_\_MPC\_O\_AL\_R02.SEN3  
 S3A\_OL\_1\_CAL\_AX\_20160523T100851\_20160530T102711\_20170426T171557\_\_\_\_\_MPC\_O\_AL\_R02.SEN3  
 S3A\_OL\_1\_CAL\_AX\_20160530T102711\_20160606T104537\_20170426T171557\_\_\_\_\_MPC\_O\_AL\_R02.SEN3  
 S3A\_OL\_1\_CAL\_AX\_20160606T104537\_20160613T110409\_20170426T171557\_\_\_\_\_MPC\_O\_AL\_R02.SEN3  
 S3A\_OL\_1\_CAL\_AX\_20160613T110409\_20160620T112246\_20170426T171557\_\_\_\_\_MPC\_O\_AL\_R02.SEN3  
 S3A\_OL\_1\_CAL\_AX\_20160620T112246\_20160627T114128\_20170426T171557\_\_\_\_\_MPC\_O\_AL\_R02.SEN3  
 S3A\_OL\_1\_CAL\_AX\_20160627T114128\_20160704T101917\_20170426T171557\_\_\_\_\_MPC\_O\_AL\_R02.SEN3  
 S3A\_OL\_1\_CAL\_AX\_20160704T101917\_20160722T004742\_20170426T171557\_\_\_\_\_MPC\_O\_AL\_R02.SEN3



## Sentinel-3 MPC

### S3-A OLCI Cyclic Performance Report

Cycle No. 017

Ref.: S3MPC.ACR.PR.01-017

Issue: 1.0

Date: 24/05/2017

Page: 23

S3A\_OL\_1\_CAL\_AX\_20160722T004742\_20160808T014848\_20170426T171557 MPC\_O\_AL\_R02.SEN3  
S3A\_OL\_1\_CAL\_AX\_20160808T014848\_20160827T170709\_20170426T171557 MPC\_O\_AL\_R02.SEN3  
S3A\_OL\_1\_CAL\_AX\_20160827T170709\_20160909T094722\_20170426T171557 MPC\_O\_AL\_R02.SEN3  
S3A\_OL\_1\_CAL\_AX\_20160909T094722\_20160923T102636\_20170426T171557 MPC\_O\_AL\_R02.SEN3  
S3A\_OL\_1\_CAL\_AX\_20160923T102636\_20161007T092447\_20170426T171557 MPC\_O\_AL\_R02.SEN3  
S3A\_OL\_1\_CAL\_AX\_20161007T092447\_20161021T100350\_20170426T171557 MPC\_O\_AL\_R02.SEN3  
S3A\_OL\_1\_CAL\_AX\_20161021T100350\_20161104T190739\_20170426T171557 MPC\_O\_AL\_R02.SEN3  
S3A\_OL\_1\_CAL\_AX\_20161104T190739\_20161117T064426\_20170426T171557 MPC\_O\_AL\_R02.SEN3  
S3A\_OL\_1\_CAL\_AX\_20161117T064426\_20161122T061449\_20170426T171557 MPC\_O\_AL\_R02.SEN3  
S3A\_OL\_1\_CAL\_AX\_20161122T061449\_20161129T145852\_20170426T171557 MPC\_O\_AL\_R02.SEN3  
S3A\_OL\_1\_CAL\_AX\_20161129T145852\_20161207T062647\_20170426T171557 MPC\_O\_AL\_R02.SEN3  
S3A\_OL\_1\_CAL\_AX\_20161207T062647\_20161210T064921\_20170426T171557 MPC\_O\_AL\_R02.SEN3  
S3A\_OL\_1\_CAL\_AX\_20161210T064921\_20161225T084146\_20170426T171557 MPC\_O\_AL\_R02.SEN3  
S3A\_OL\_1\_CAL\_AX\_20161225T084146\_20170110T082623\_20170426T171557 MPC\_O\_AL\_R02.SEN3  
S3A\_OL\_1\_CAL\_AX\_20170110T082623\_20170124T122451\_20170426T171557 MPC\_O\_AL\_R02.SEN3  
S3A\_OL\_1\_CAL\_AX\_20170124T122451\_20170214T145948\_20170426T171557 MPC\_O\_AL\_R02.SEN3  
S3A\_OL\_1\_CAL\_AX\_20170214T145948\_20170227T123949\_20170426T171557 MPC\_O\_AL\_R02.SEN3  
S3A\_OL\_1\_CAL\_AX\_20170227T123949\_20170312T083848\_20170426T171557 MPC\_O\_AL\_R02.SEN3  
S3A\_OL\_1\_CAL\_AX\_20170312T083848\_20170322T142139\_20170426T171557 MPC\_O\_AL\_R02.SEN3  
S3A\_OL\_1\_CAL\_AX\_20170322T142139\_20170331T184952\_20170426T171557 MPC\_O\_AL\_R02.SEN3  
S3A\_OL\_1\_CAL\_AX\_20170331T184952\_20170413T094608\_20170426T171557 MPC\_O\_AL\_R02.SEN3  
S3A\_OL\_1\_CAL\_AX\_20170413T094608\_20170420T233158\_20170426T171557 MPC\_O\_AL\_R02.SEN3  
S3A\_OL\_1\_CAL\_AX\_20170420T233158\_20991231T235959\_20170426T171557 MPC\_O\_AL\_R02.SEN3

This set of ADFs is intended to be used first (and further validated) in a coming partial reprocessing dedicated to the validation of Level 2 processing evolutions. If validated it would be ready for use for a global reprocessing and the last one could be used for NRT processing, with a different referencing (yet to be defined).

### 1.2.5 Radiometric Calibrations for sun azimuth angle dependency and Yaw Manoeuvres for Solar Diffuser on-orbit re-characterization [OLCI-L1B-CV-270 and OLCI-L1B-CV-280]

This activity has not evolved during cycle 017 and results presented in previous report are still valid.

## 1.3 Spectral Calibration [OLCI-L1B-CV-400]

There has been no Spectral Calibration acquisition during cycle 017.

## 1.4 Signal to Noise assessment [OLCI-L1B-CV-620]

### 1.4.1 SNR from Radiometric calibration data.

SNR computed for all calibration data as a function of band number is presented in Figure 27.

SNR computed for all calibration data as a function of orbit number for band Oa01 (the less stable band) is presented in Figure 28.



**Sentinel-3 MPC**  
**S3-A OLCI Cyclic Performance Report**  
**Cycle No. 017**

Ref.: S3MPC.ACR.PR.01-017  
 Issue: 1.0  
 Date: 24/05/2017  
 Page: 24

There is no significant evolution of this parameter during the current cycle and the ESA requirement is fulfilled for all bands.

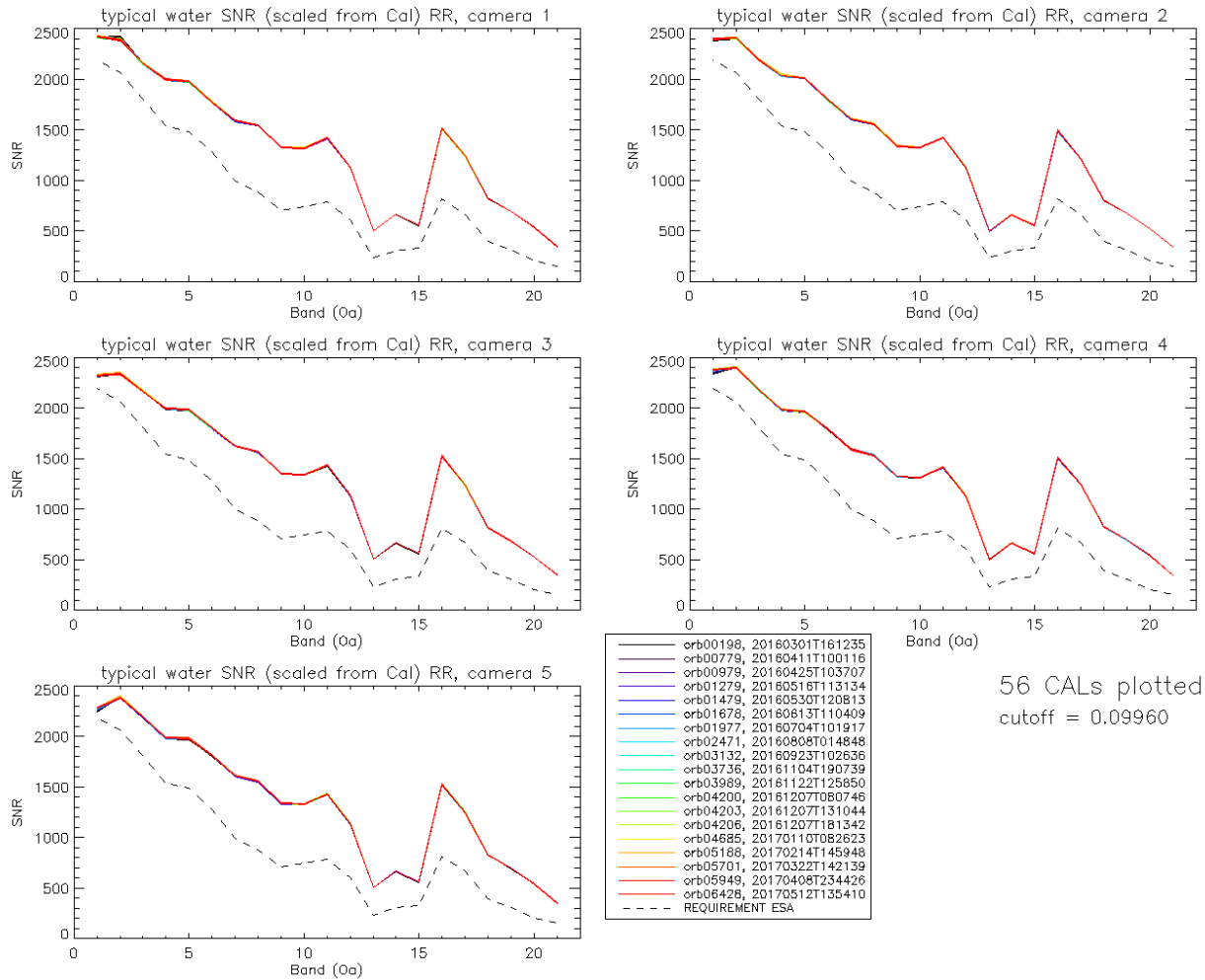


**Figure 27: Signal to Noise ratio as a function of the spectral band for the 5 cameras. These results have been computed from radiometric calibration data. All calibrations except first one (orbit 183) are presents with the colours corresponding to the orbit number (see legend). The SNR is very stable with time: the curves for all orbits are almost superimposed. The dashed curve is the ESA requirement.**

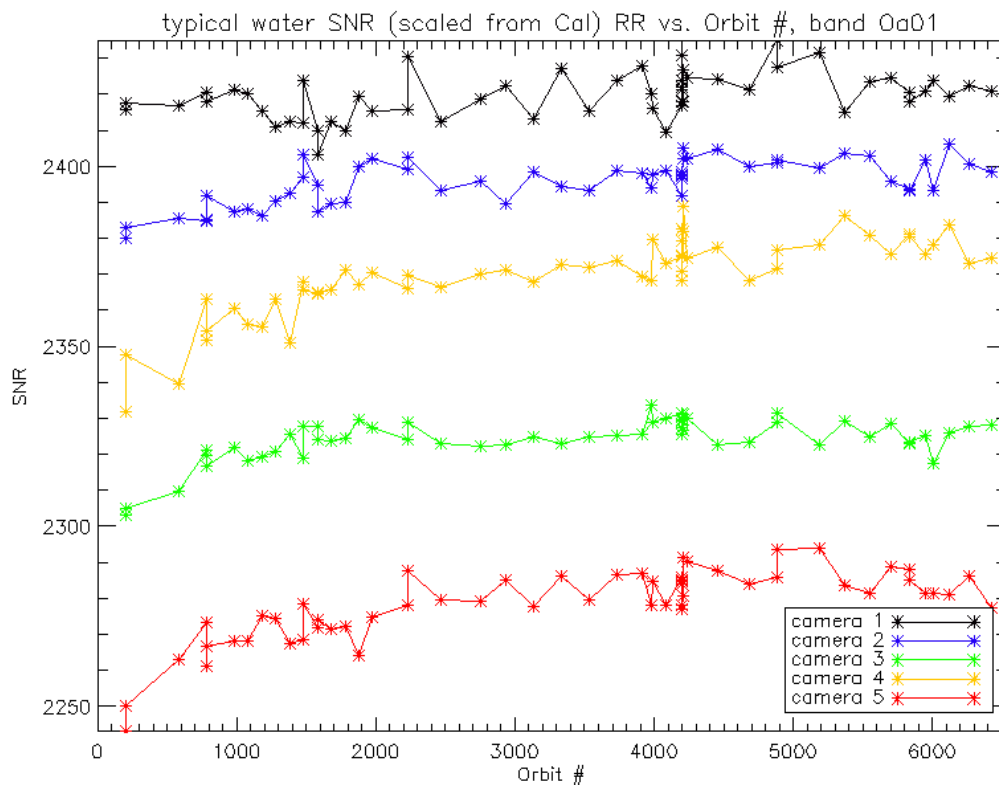


Figure 28: long-term stability of the SNR estimates from Calibration data, example of channel Oa1.

### 1.4.2 SNR from EO data.

There has been no update on SNR assessment from EO data during the cycle. Last figures (cycle 9) are considered valid.

## 1.5 Geometric Calibration/Validation

The Validation version GeoCal Tool implemented within the MPMF is now operational and used to monitor OLCI geometric performance. April's results show very good performance. Monitoring of the geolocation performance by correlation with GCP imageries using the GeoCal tool over the period confirms that OLCI is compliant with its requirement: the centroid of the geolocation error is around 0.2 pixel in both along-track and across-track directions (Figure 29: histograms of geolocation errors for the along-track (left) and across-track (right) directions).

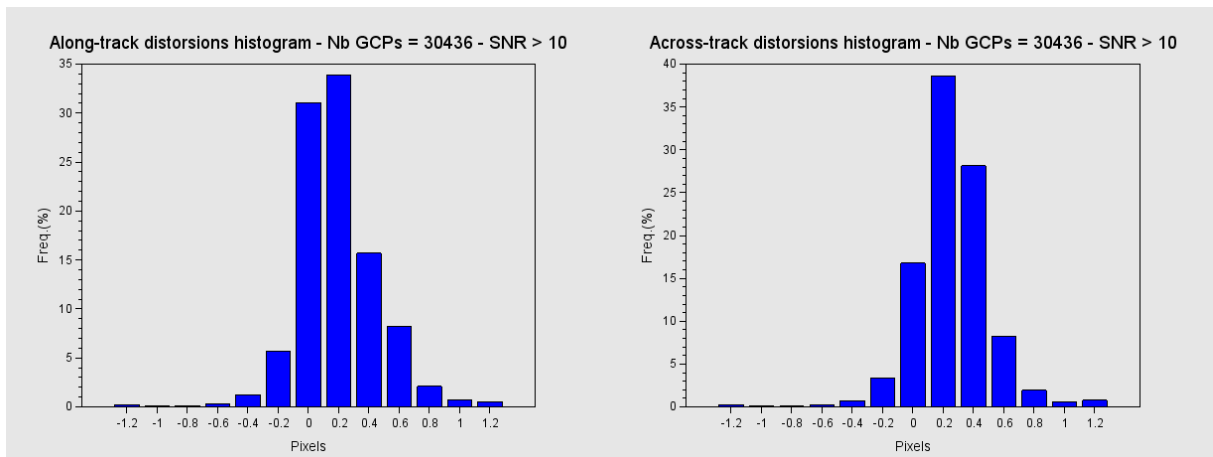


**Figure 29: histograms of geolocation errors for the along-track (left) and across-track (right) directions.**

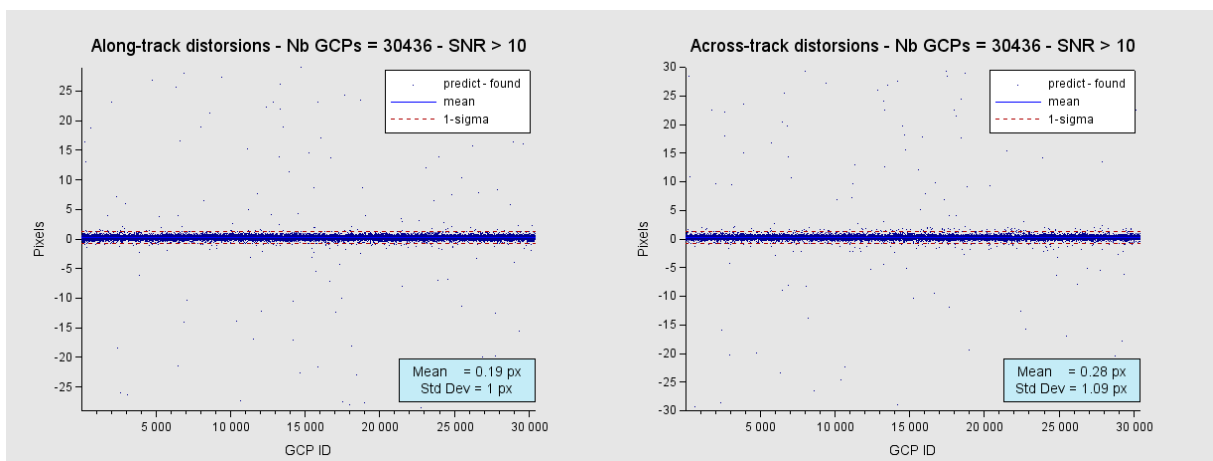


**Figure 30: georeferencing error in along-track (left) and across-track (right) directions for all the GCPs.**

The series plots of along-track and across-track georeferencing errors (Figure 30) show the pretty good stability of the geometric calibration but also highlight the significant number of outliers, despite the filtering on correlation level (SNR). This is further highlighted by plots of Figure 31 to Figure 33, each showing geolocation error estimates for restricted periods of 2 days spread over current cycle.

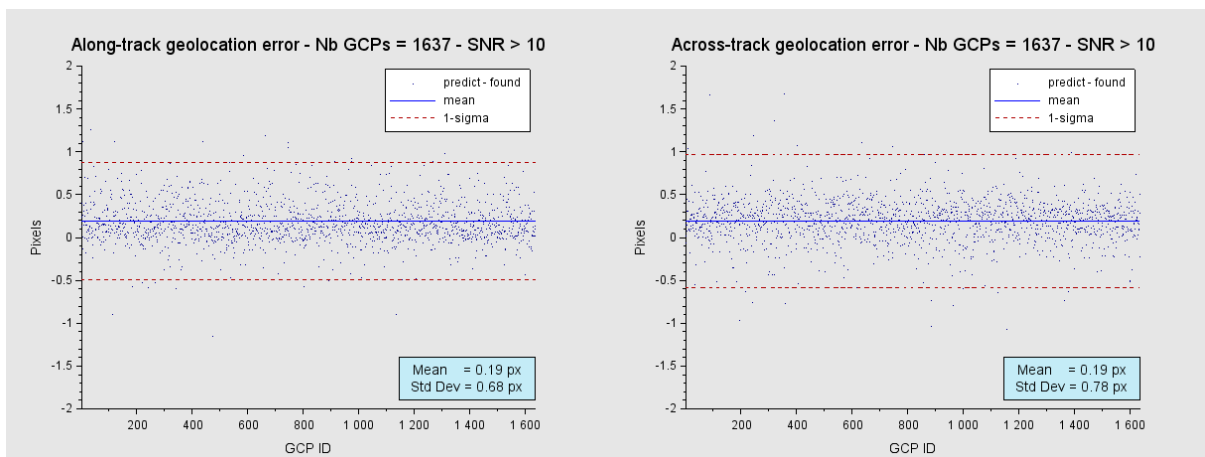


Figure 31: same as Figure 30 for 23<sup>rd</sup> and 24<sup>th</sup> of April, with a restricted vertical scale.

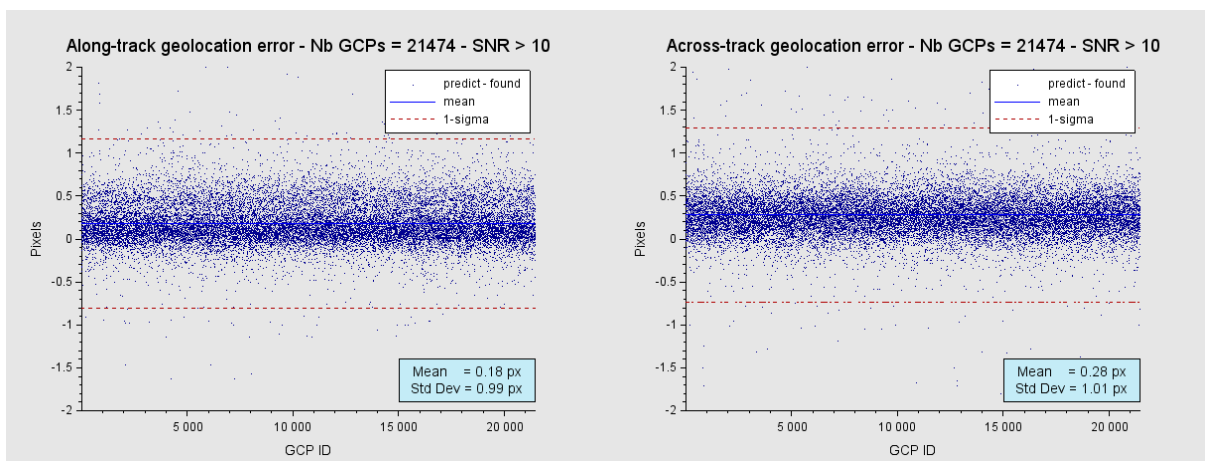


Figure 32: same as Figure 30 for 3<sup>rd</sup> and 4<sup>th</sup> of May, with a restricted vertical scale.

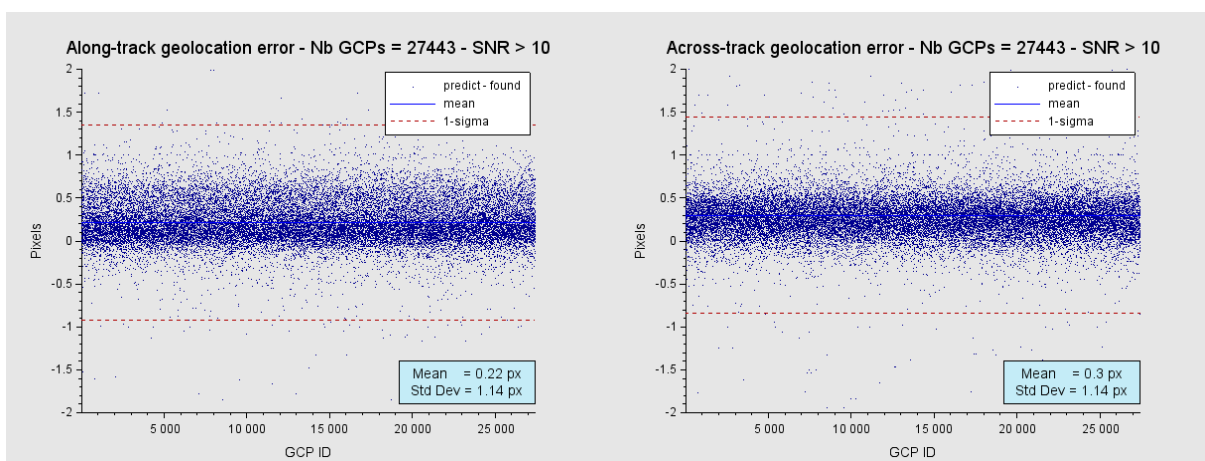


Figure 33: same as Figure 30 for 14<sup>th</sup> and 15<sup>th</sup> of May, with a restricted vertical scale.

	<p><b>Sentinel-3 MPC</b></p> <p><b>S3-A OLCI Cyclic Performance Report</b></p> <p><b>Cycle No. 017</b></p>	<p>Ref.: S3MPC.ACR.PR.01-017</p> <p>Issue: 1.0</p> <p>Date: 24/05/2017</p> <p>Page: 28</p>
--	--	--

## 2 OLCI Level 1 Product validation

**[OLCI-L1B-CV-300], [OLCI-L1B-CV-310] – Radiometric Validation**

### **S3ETRAC Service**

#### **Activities done**

The S3ETRAC service extracts OLCI L1 RR and SLSTR L1 RBT data and computes associated statistics over 49 sites corresponding to different surface types (desert, snow, ocean maximizing Rayleigh signal, ocean maximizing sunglint scattering and deep convective clouds). The S3ETRAC products are used for the assessment and monitoring of the L1 radiometry (optical channels) by the ESLs.

All details about the S3ETRAC/OLCI and S3ETRAC/SLSTR statistics are provided on the S3ETRAC website <http://s3etrac.acri.fr/index.php?action=generalstatistics>

- ❖ Number of OLCI products processed by the S3ETRAC service
- ❖ Statistics per type of target (DESERT, SNOW, RAYLEIGH, SUNGLINT and DCC)
- ❖ Statistics per sites
- ❖ Statistics on the number of records

For illustration, we provide below statistics on the number of S3ETRAC/OLCI records generated per type of targets (DESERT, SNOW, RAYLEIGH, SUNGLINT and DCC).

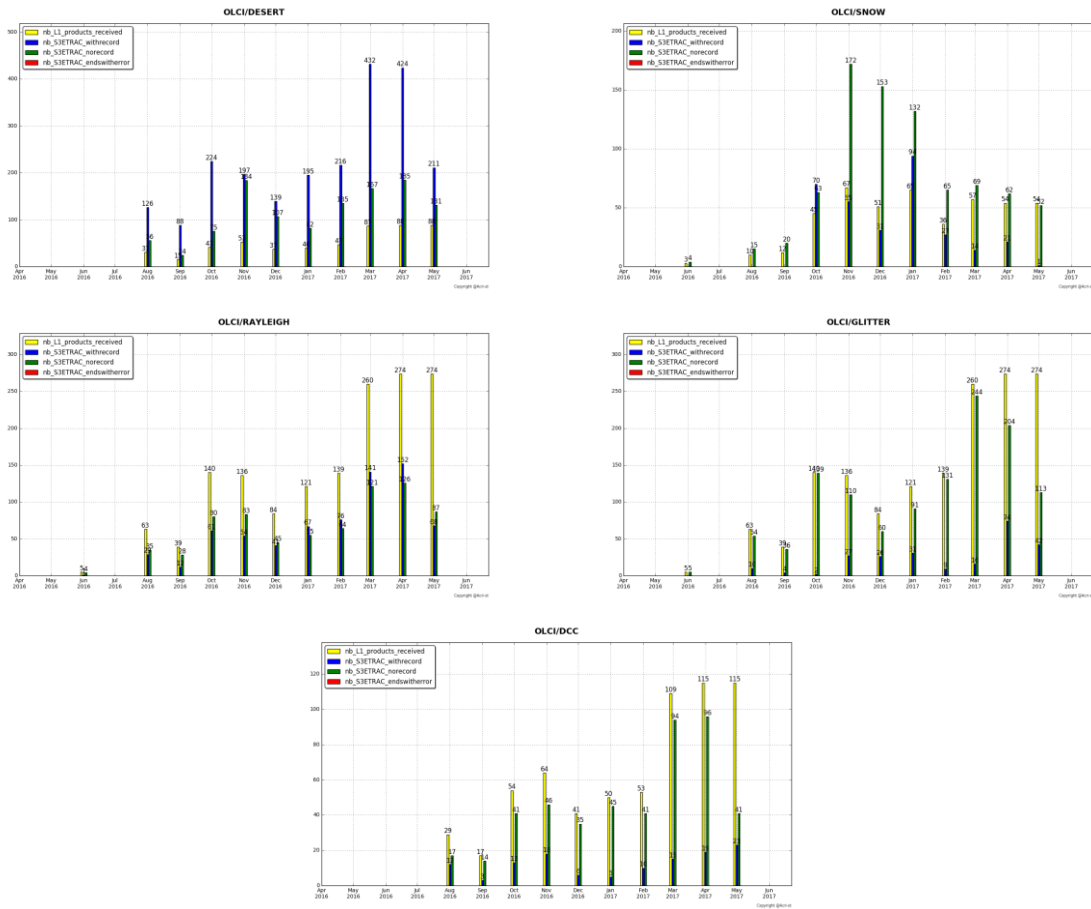


**Figure 34: summary of S3ETRAC products generation for OLCI**  
 (number of OLCI L1 products Ingested, yellow – number of S3ETRAC extracted products generated, blue – number of S3ETRAC runs without generation of output product (data not meeting selection requirements), green – number of runs ending in error, red, one plot per site type).

**Radiometric validation with DIMITRI**

**Highlights**

- Run Rayleigh and Glint methods over the available mini-file (ROIs) until May 2017 from ERR-LN1 products.
- Analysis of OLCI results over Glint and Rayleigh has been performed over the indicated periods (September 2016 – May 2017).
- The results are consistent with the Desert calibration results and attest the improvement of the L1B-radiometry quality since September 2016, where the biases over Oa05-Oa12 are within the mission requirements (2%), while Oa01-Oa4 (Rayleigh) and Oa16, Oa17 and Oa18 (Glint) show biases of 3%.
- The main issue is the lack of mini-files over DIMITRI-ROIs.

**I-Validation over PICS**



**Sentinel-3 MPC**  
**S3-A OLCI Cyclic Performance Report**  
**Cycle No. 017**

Ref.: S3MPC.ACR.PR.01-017  
 Issue: 1.0  
 Date: 24/05/2017  
 Page: 30

**PICS method:**

The ingestion of the l1b time-series over the six desert CalVal sites; from LN1\_O\_NT products has been extended until 18<sup>th</sup> May 2017. The whole dataset has been ingested successfully into DIMITRI and automatically (manually when necessary) cloud-screened. The results are displayed below.

1. The results are consistent overall the six used PICS sites (Figure 35). OLCI reflectance shows strong fluctuation in the beginning of the commissioning phase (about  $\pm 8\%$  amplitude) between March and July 2016. The temporal average over the period **September 2016 – April 2017** of the elementary ratios (observed reflectance to the simulated one) shows values within 2% (mission requirements) over all the VNIR bands (Figure 36). The spectral bands with significant absorption from water vapour and O<sub>2</sub> (Oa11, Oa13 and Oa14) show an outlier ratio.

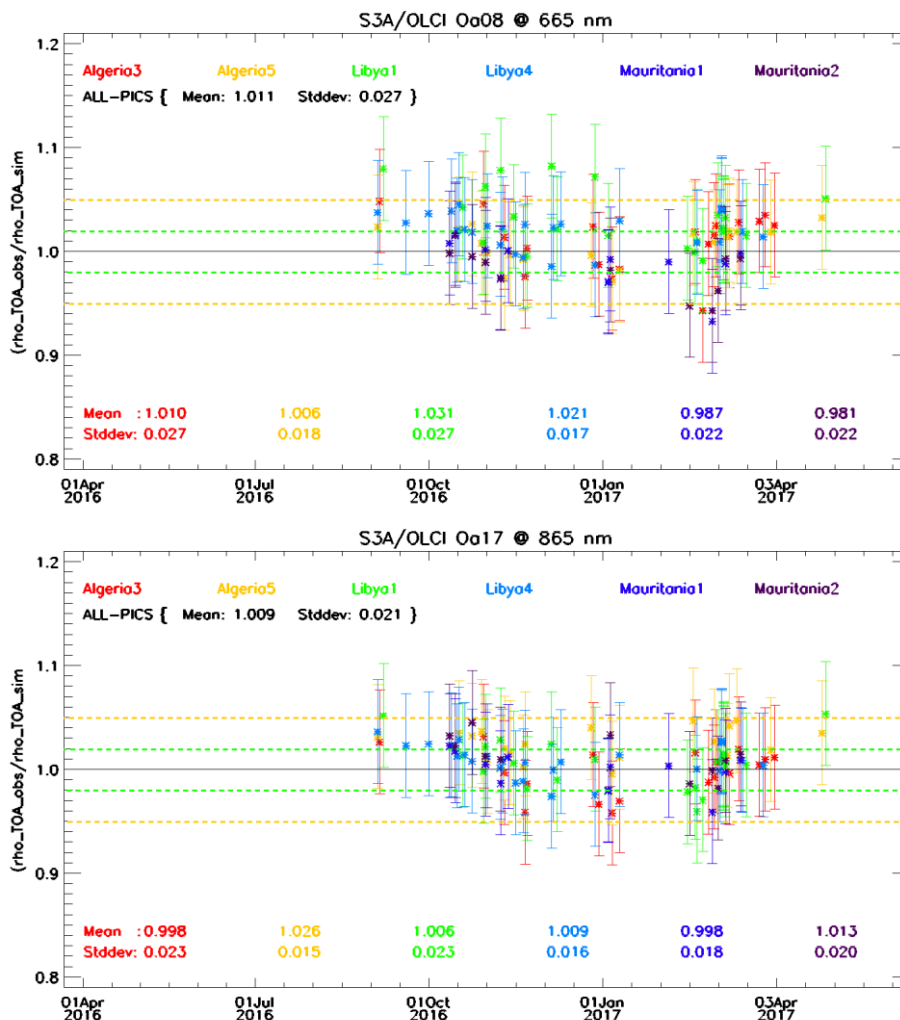


**Figure 35: Time-series of the elementary ratios (observed/simulated) signal from S3A/OLCI for (top) band Oa8 and (bottom) band Oa17 over Six PICS Cal/Val sites. Dashed-green and orange lines indicate the 2% and 5% respectively. Error bars indicate the desert methodology uncertainty.**

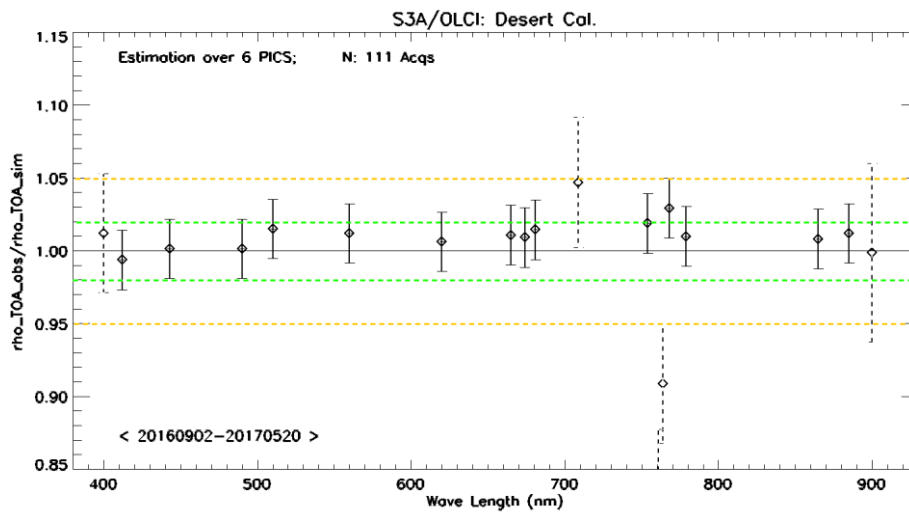


Figure 36: The estimated gain values for S3A/OLCI over the 6 PICS sites identified by CEOS over the period September 2016 – May 2017 as a function of wavelength. Dashed-green and orange lines indicate the 2% and 5% respectively. Error bars indicate the desert methodology uncertainty.

## II-Intercomparison S3A/OLCI, S2A/MSI and LANDSAT/OLI over PICS

1. X-mission Intercomparison with MSI-A is on-going
2. We were unable to perform the x-mission Intercomparison with MODIS-A since March 2017 due to an issue with the downloaded L1B-products following to changes on the website ([modis.gsfc.nasa.gov](http://modis.gsfc.nasa.gov)).

## III-Validation over Rayleigh

The investigations of the discrepancy between the results from ARGANS and ESTEC, when both use the same CFI (DIMITRI), have been done. Following to several email exchanges with Marc Bouvet (ESTEC) then personal meeting during the RadCalNet workshop, we found that ARGANS and ESTEC have used different thresholds over Rayleigh in DIMITRI. ARGANS's ESL has performed Rayleigh using ESTEC-thresholds over the period September 2016-March 2017. We found slightly different results due to the different used period. The outcome of this analysis will be provided to the S3MPC in a separate TN soon.

Rayleigh method has been run on the CTCP over the available mini-files on the Opt-server. The results produced with the configuration (ROI-AVERAGE) are consistent with the previous results. Note that it has been admitted that DIMITRI gives about 1%-2% higher gain, mainly over bands <500 nm (Figure 37).

## IV-Validation over Glint

Glint calibration method (DIMITRI; PIXEL-Option) has been performed over the period September 2016 – May 2017 from the available mini-files. The outcome of this analysis shows a good consistency with the desert outputs (see Figure 37). In addition it attests the improvement of the radiometry quality of OLCI after November 2016.

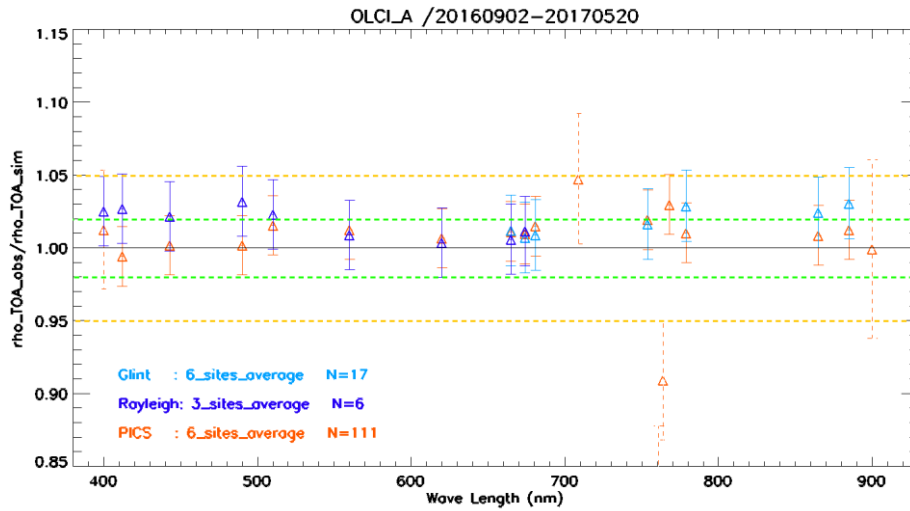


**Figure 37: The estimated gain values for S3A/OLCI from Glint, Rayleigh, and PICS over the period September 2016 – May 2017 as a function of wavelength. We use the gain value of Oa8 from Desert method as reference gain for Glint. Dashed-green and orange lines indicate the 2% and 5% respectively. Error bars indicate the methods uncertainties.**

**Radiometric validation with OSCAR**

The S3ETRAC Rayleigh scenes of February 2017 over 4 sites (AtIN, IndS, PacN and PacSE) have been processed, processing of other sites and of March scenes is on-going. Corresponding results are shown on Figure 38.

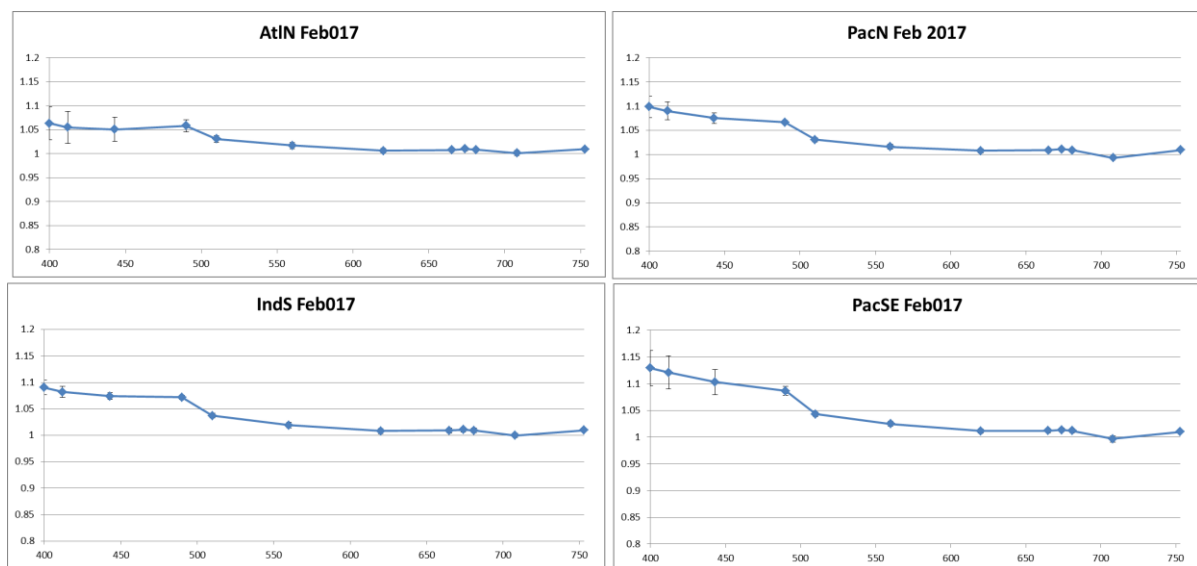


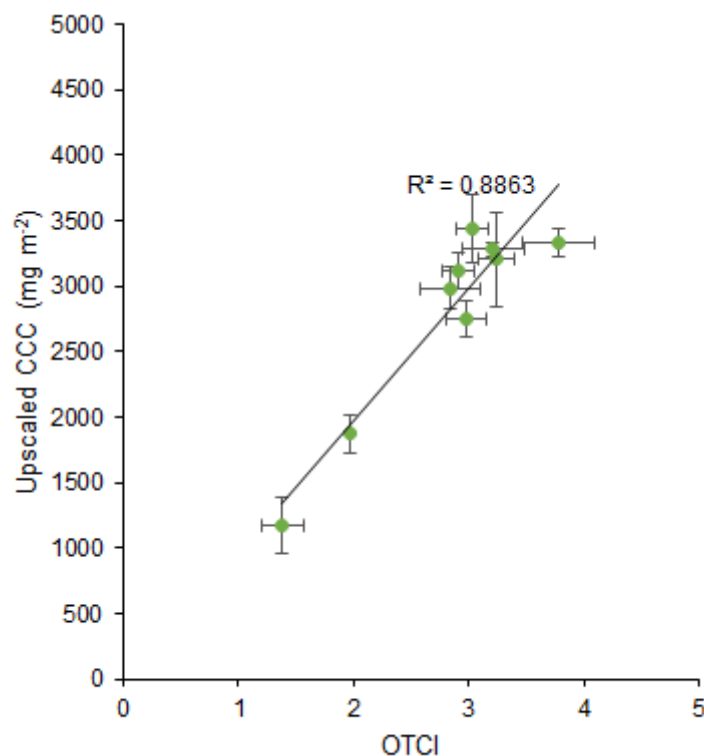
**Figure 38 Oscar Rayleigh results for February 2017 for AtIN, IndS, PacN and PacSE sites.**



### 3 Level 2 Land products validation

#### [OLCI-L2LRF-CV-300]

To provide data against which the OLCI L2 products could be validated, a series of field campaigns were carried out over a 1 km<sup>2</sup> area of the deciduous broadleaf forest UK-NFo site during 2016. By collecting measurements on dates throughout the year, the performance of the OTCI at a wide range of CCC values could be evaluated. Measurements of canopy chlorophyll content (CCC) were obtained in 9 elementary sampling units of 40 m x 40 m. Estimates of leaf area index (LAI) were obtained using digital hemispherical photography (DHP), whilst estimates of leaf chlorophyll concentration (LCC) were obtained using an optical chlorophyll meter. Relative values were converted to absolute LCC using previously published calibration equations. The product of these LAI and LCC variables provided estimates of CCC at the ESU level. Collected in-situ measurements were upscaled to the 300 m spatial resolution of OLCI using Sentinel-2 Multispectral Instrument (MSI) data. Several upscaling options were considered, including the use of the L2B processor incorporated within the Sentinel Applications Platform (SNAP), which uses an artificial neural network (ANN) trained over radiative transfer model (RTM) simulations to retrieve biophysical variables from MSI data. However, a spectral vegetation index similar to the OTCI provided a stronger relationship with in-situ CCC, so an empirical transfer function was adopted. Upscaled maps of CCC were compared with near-contemporaneous OLCI L2 products, after cloud and quality flags were applied. Good performance was demonstrated by a strong linear relationship between the OTCI and upscaled CCC ( $R^2 = 0.89$ ).



Relationship between the OTCI and CCC upscaled from in-situ measurements using MSI data.



**Sentinel-3 MPC**  
**S3-A OLCI Cyclic Performance Report**  
**Cycle No. 017**

Ref.: S3MPC.ACR.PR.01-017  
Issue: 1.0  
Date: 24/05/2017  
Page: 34

A series of additional field campaigns for OLCI L2 validation are planned between June and August 2017 over both the vineyard SP-Val and broadleaf deciduous forest UK-NFo sites. The differing vegetation types will enable product performance to be assessed over canopies with diverse structural and biophysical characteristics. These field campaigns will be carried out over a larger 10 km<sup>2</sup> area, providing a greater amount of data for validation and enabling a wider range of biophysical variable values to be represented. Using the protocols adopted in the 2016 campaigns, in-situ measurements will be made to provide data against which the OGVI and OTCI can be validated. During each campaign, airborne hyperspectral data will be collected by the Natural Environment Research Council (NERC) Airborne Research Facility (ARF) to facilitate the upscaling of in-situ data to the 300 m spatial resolution of OLCI, making use of the Specim AISAfenix instrument. It's high spatial (1.52 m at 1000 m above ground level) and spectral (3.5 nm full-width half-maximum) resolution makes it well-suited to this task. Using the airborne hyperspectral data as a reference, a more rigorous assessment of the potential of MSI data for upscaling will be carried out.



Planned flight lines covering the SP-Val (top) and UK-NFo (bottom) site.

	<p><b>Sentinel-3 MPC</b></p> <p><b>S3-A OLCI Cyclic Performance Report</b></p> <p><b>Cycle No. 017</b></p>	<p>Ref.: S3MPC.ACR.PR.01-017</p> <p>Issue: 1.0</p> <p>Date: 24/05/2017</p> <p>Page: 35</p>
--	--	--

**[OLCI-L2LRF-CV-410 & OLCI-L2LRF-CV-420] – Cloud Masking & Surface Classification for Land Products**

There has been no update on Land Cloud Masking & Surface Classification validation quantitative assessment during the cycle. Last figures (cycle 10) are considered valid.

Qualitative assessment by product inspection showed no detectable performance evolution.

**Validation of Integrated Water Vapour over Land**

There has been no update on Integrated Water Vapour over Land validation quantitative assessment during the cycle. Last figures (cycle 15) are considered valid.

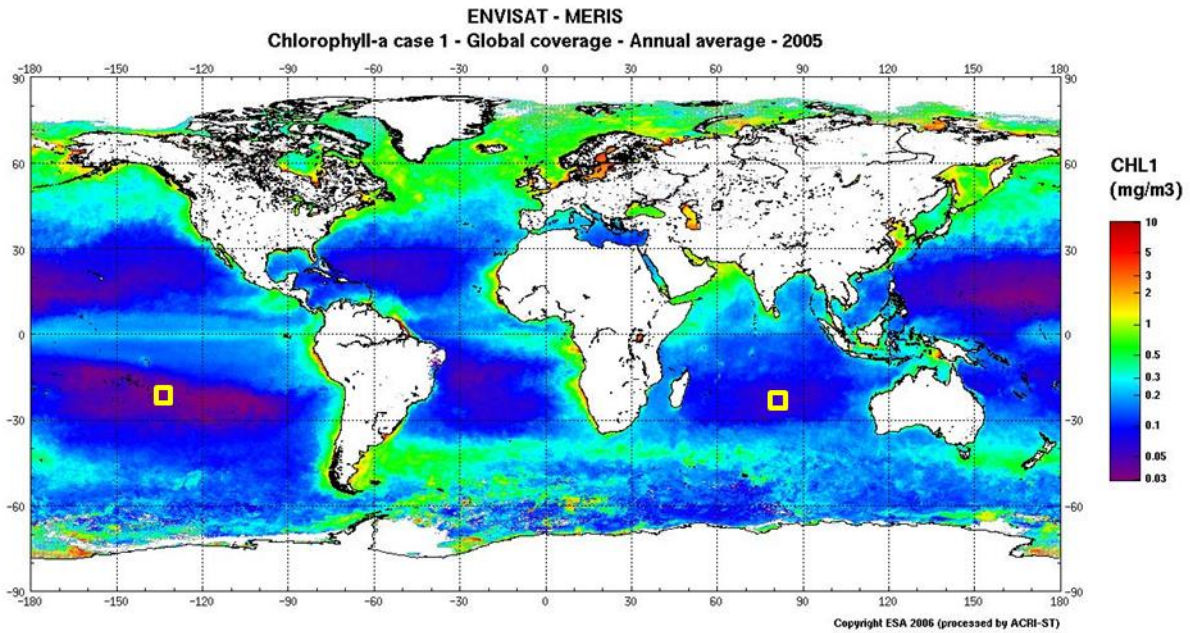
Qualitative assessment by product inspection showed no detectable performance evolution.



## 4 Level 2 Water products validation

### 4.1.1.1 [OLCI-L2-CV-210, OLCI-L2-CV-220] – Vicarious calibration of the NIR and VIS bands

On the basis of reprocessed data using the recent Instrument Gain model (see section 1.2), time series over the South Indian Ocean (SIO) and South Pacific Gyre (SPG) have been used to compute the NIR gains (figure below).



In both NIR and visible gain calculation procedures, the strategy consist in avoiding glint. In oligotrophic areas, the marine signal can be considered as null so that the resulting equation is in single scattering approximation:

$$\rho_{TOA}^{NIR}(\lambda) = \rho_{path}^{NIR}(\lambda) + t(\lambda) * \rho_{purewater}^{NIR}(\lambda) = \rho_{aer}^{NIR}(\lambda) + \rho_{rayleigh}^{NIR}(\lambda) + t(\lambda) * \rho_{purewater}^{NIR}(\lambda)$$

The strategy consists in computing individual gains over the entire time series. Over the NIR spectrum, a linear fit of the log of the aerosol reflectance to the log of the wavelength is used to compute a theoretical  $\rho_{aer}^T(\lambda)$ . This is possible by excluding 1020nm band, the other bands being already quite well spectrally aligned. Note this procedure does not make any assumption of any aerosol model nor reference NIR band.

Individual gains are calculated as follow:

$$G_i(\lambda) = \frac{\rho_{TOA}^T(\lambda)}{\rho_{TOA}(\lambda)}$$

$$\rho_{TOA}^T(\lambda) = \rho_{aer}^T(\lambda) + \rho_{rayleigh}(\lambda) + t(\lambda) * \rho_{purewater}^{NIR}(\lambda)$$

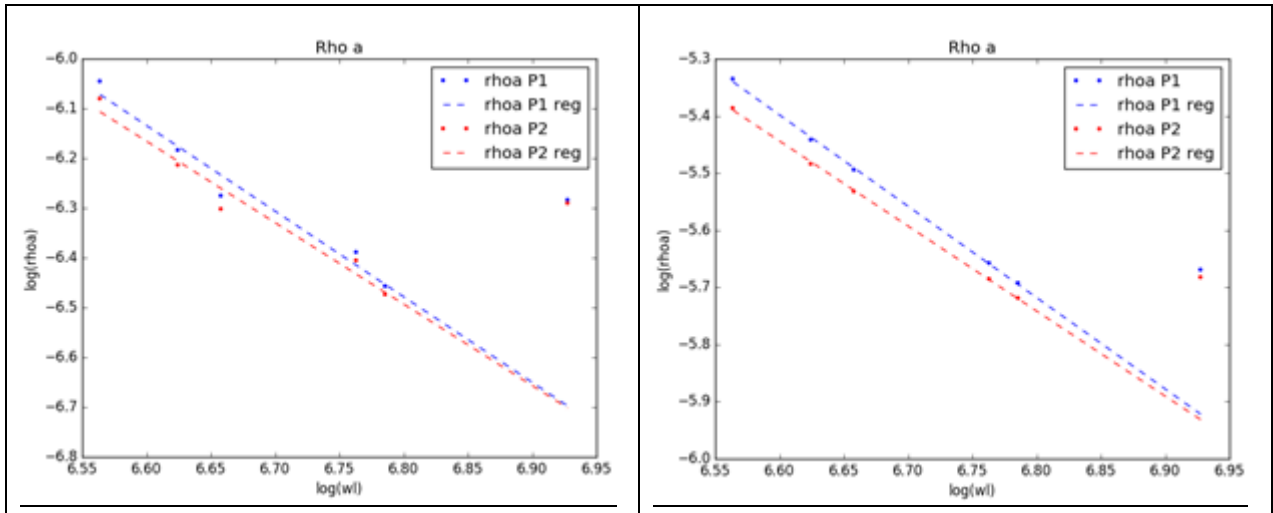
$$\rho_{aer}^T(\lambda) = e^{a * \log(\lambda) + b}$$

With a and b the slope and intercept respectively of the linear fine between  $\log(\rho_{aer}^T(\lambda))$  and  $\log(\lambda)$   $\lambda = [709, 754, 779, 865, 885]$ . See exemple of single pixel regression below:

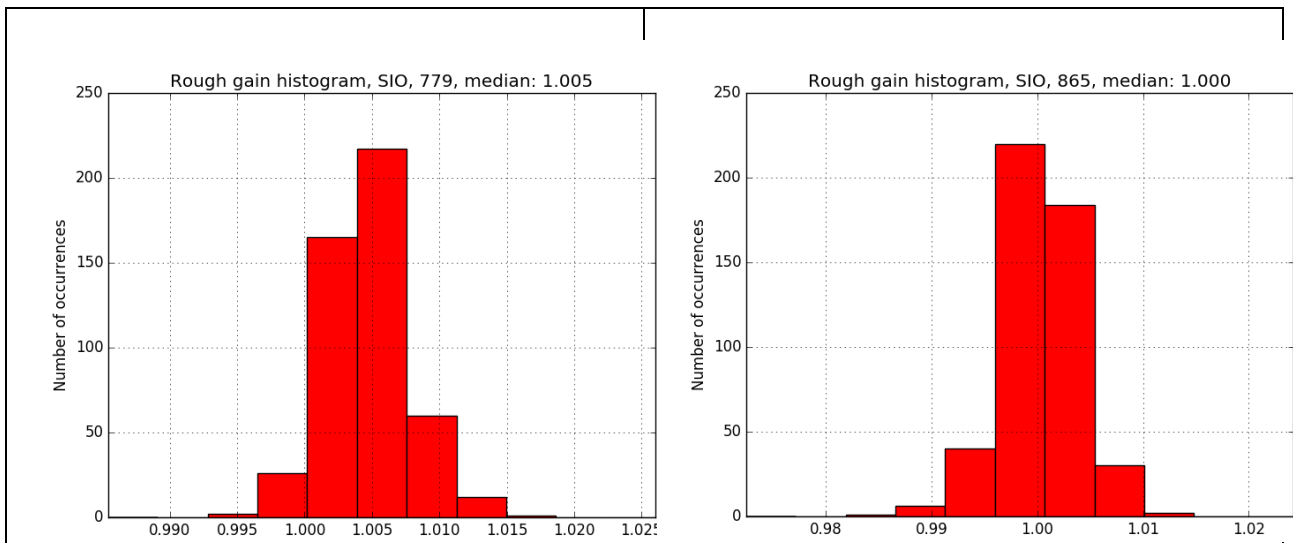


**Sentinel-3 MPC**  
**S3-A OLCI Cyclic Performance Report**  
**Cycle No. 017**

Ref.: S3MPC.ACR.PR.01-017  
 Issue: 1.0  
 Date: 24/05/2017  
 Page: 37



A macro pixel gain time series is then derived as the median of each macropixel.  
 The final gain is computed as the median of the gain time series.  
 Histograms below show the distribution of



Final NIR gains are listed in the table below:

Site/band	709	754	779	865	885	1020
SIO/SPG mean	0.996	1.003	1.005	1.000	0.996	0.914

In a second step, visible bands vicarious gain have been computed using BOUSSOLE MOBY and globcolour climatologies to increase the number of data to derived gains.

$$\rho_{TOA}^{VIS}(\lambda) = \rho_{path}^{VIS}(\lambda) + t(\lambda) * \rho_w^{VIS}(\lambda) = \rho_{aer}^{VIS}(\lambda) + \rho_{rayleigh}^{VIS}(\lambda) + t(\lambda) * \rho_w^{VIS}(\lambda)$$



$$G_i(\lambda) = \frac{\rho_{TOA}^T(\lambda)}{\rho_{TOA}(\lambda)}$$

$$\rho_{TOA}^T(\lambda) = \rho_{aer}^{vis}(\lambda) + \rho_{rayleigh}^{vis}(\lambda) + t(\lambda) * \rho_{wIS}^{vis}(\lambda)$$

In the current processin branch two water leavin reflectances are calculated at 2 bracketing pressure  $\rho_{wIS}^{vis P1}(\lambda)$  and  $\rho_{wIS}^{vis P2}(\lambda)$ .

$\rho_{wIS}^{vis P1}(\lambda) = \frac{\rho_{TOA}^{P1}(\lambda) - \rho_{path}^{P1}(\lambda)}{t^{P1}(\lambda)}$	$\rho_{wIS}^{vis P2}(\lambda) = \frac{\rho_{TOA}^{P2}(\lambda) - \rho_{path}^{P2}(\lambda)}{t^{P2}(\lambda)}$
---	---

$$\rho_w^{vis}(\lambda) = (1 - \varepsilon)\rho_{wIS}^{vis P1}(\lambda) + \varepsilon\rho_{wIS}^{vis P2}(\lambda) \text{ with } \varepsilon = \frac{P_1 - P_{ECMWF}}{P_1 - P_2}$$

$$G_i(\lambda) = \frac{\rho_{wIS}^{vis}(\lambda) + (1 - \varepsilon)\frac{\rho_{path}^{P1}(\lambda)}{t^{P1}(\lambda)} + \varepsilon\frac{\rho_{path}^{P2}(\lambda)}{t^{P2}(\lambda)}}{(1 - \varepsilon)\frac{\rho_{TOA}^{P1}(\lambda)}{t^{P1}(\lambda)} + \varepsilon\frac{\rho_{TOA}^{P2}(\lambda)}{t^{P2}(\lambda)}}$$

At a pressure node:

$$G_i(\lambda) = \frac{t(\lambda)\rho_{wIS}^{vis}(\lambda) + \rho_{path}^{vis}(\lambda)}{\rho_{TOA}^{vis}(\lambda)}$$

By construction after adjustment,

$$(1 - \varepsilon)\rho_w^{P1}(\lambda) + \varepsilon\rho_w^{P2}(\lambda) = \rho_w^{IS}(\lambda)$$

As for NIR gain, a first matchup time series is computed as the median gain of the macropixel.

The final gain is calculated as the weighted value of each individual gains:

$$\bar{G}(\lambda) = \frac{\sum^N \frac{1}{\sigma_{Gi}} G_i}{\sum^N \frac{1}{\sigma_{Gi}}} \text{ with } \sigma_{Gi} = \sqrt{\sigma_{sat}^2 + \sigma_{IS}^2} \text{ with } \sigma_{sat} \text{ the macropixel standard deviation of the remote-sensing water-leaving reflectance and } \sigma_{IS} = 5\% \rho_{wIS}$$

Visible gain time series

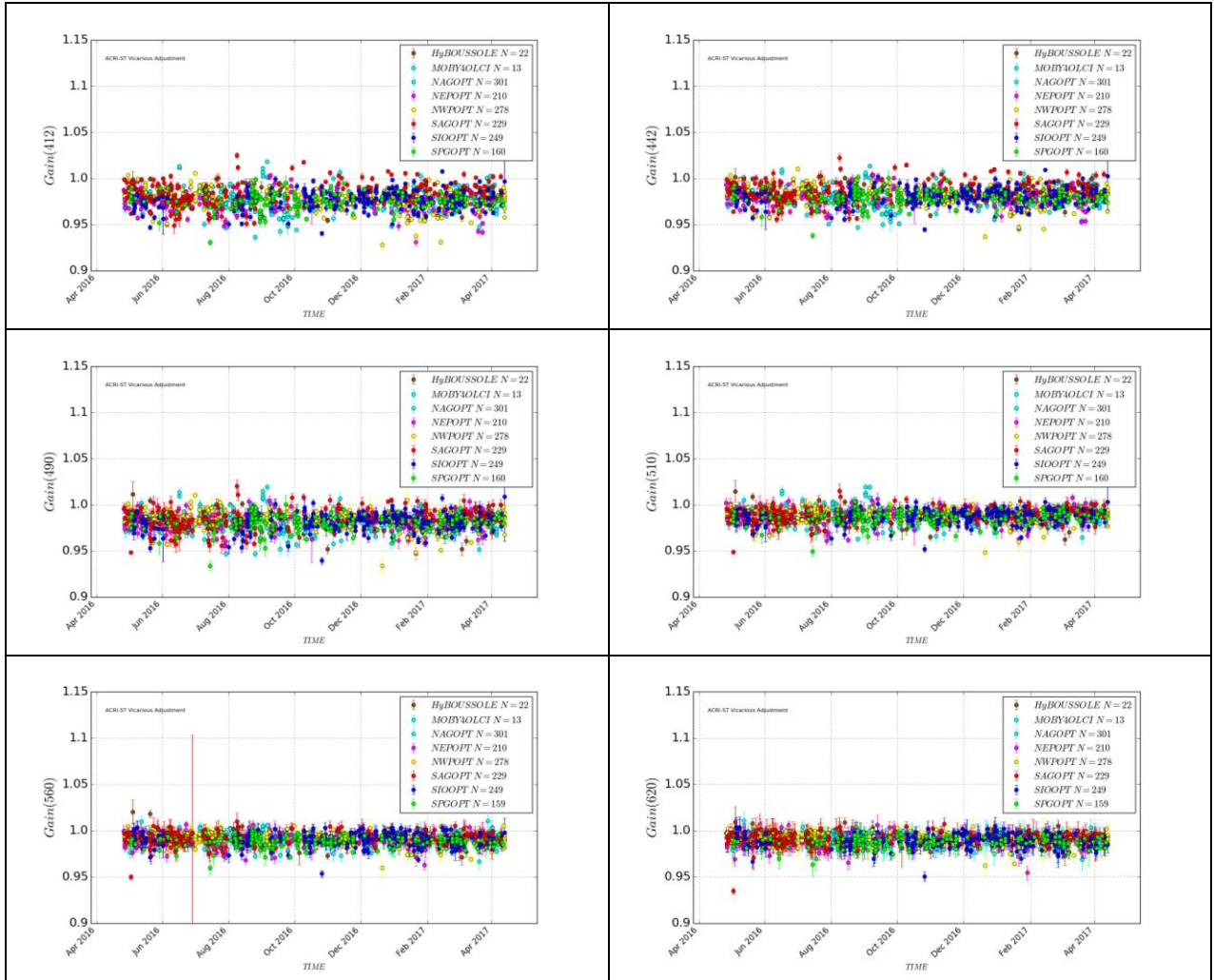


# Sentinel-3 MPC

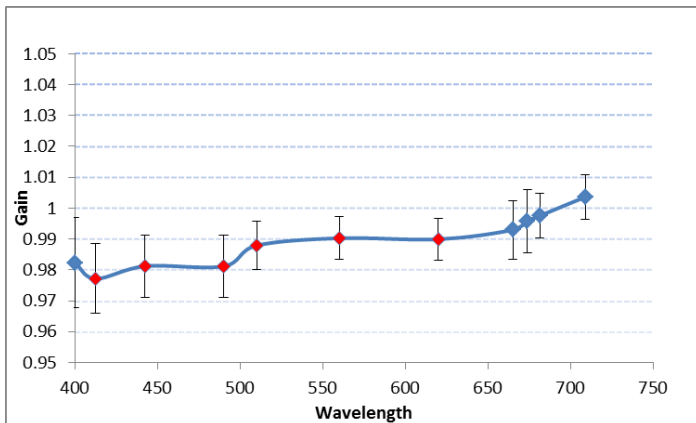
## S3-A OLCI Cyclic Performance Report

### Cycle No. 017

Ref.: S3MPC.ACR.PR.01-017  
 Issue: 1.0  
 Date: 24/05/2017  
 Page: 39



Visible gain spectrum:



Final gain set:



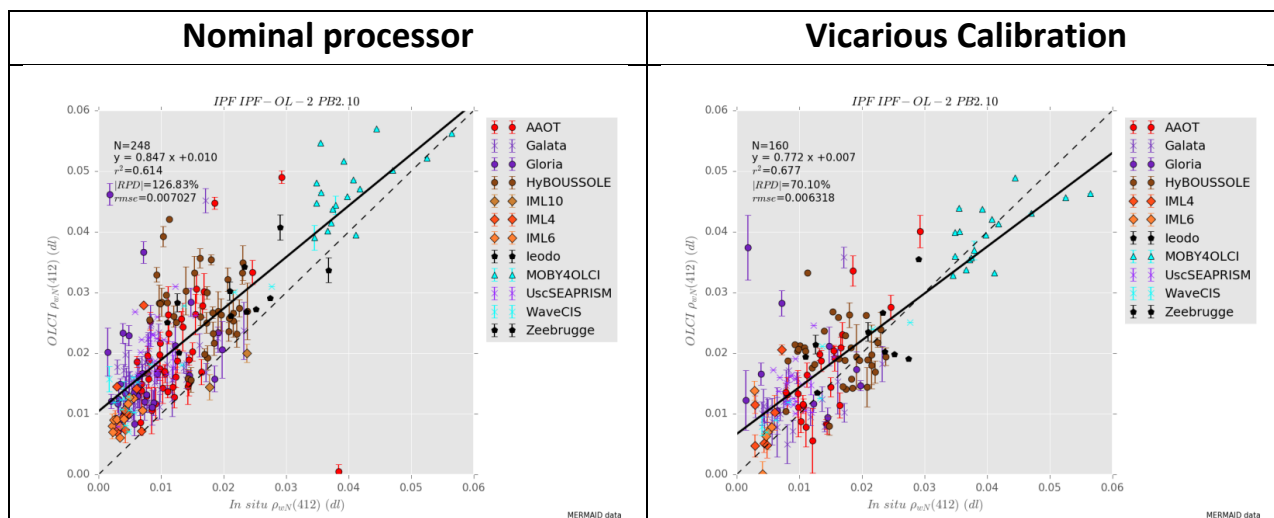
Wavelength	mean G	stds
400	0.982	0.0146
<b>412.5</b>	<b>0.977</b>	<b>0.0113</b>
<b>442.5</b>	<b>0.981</b>	<b>0.0100</b>
<b>490</b>	<b>0.981</b>	<b>0.0100</b>
<b>510</b>	<b>0.988</b>	<b>0.0078</b>
<b>560</b>	<b>0.990</b>	<b>0.0069</b>
<b>620</b>	<b>0.990</b>	<b>0.0067</b>
665	0.993	0.0095
673.75	0.996	0.0101
681.25	0.998	0.0073
708.75	1.004	0.0071

[OLCI-L2WLR-CV-300, OLCI-L2WLR-CV-310, OLCI-L2WLR-CV-32, OLCI-L2WLR-CV-330, OLCI-L2WLR-CV-340, OLCI-L2WLR-CV-350, OLCI-L2WLR-CV-360 and OLCI-L2WLR-CV-370] – Level 2 Water-leaving Reflectance product validation after implementation of vicarious gains.

Activities done

- ❖ The focus for this time period has been on the validation of the Vicarious Gain implementation.
- ❖ All extractions and statistics have been regenerated for the whole mission (April 26<sup>th</sup> 2016 onward, restricted to validation sites).

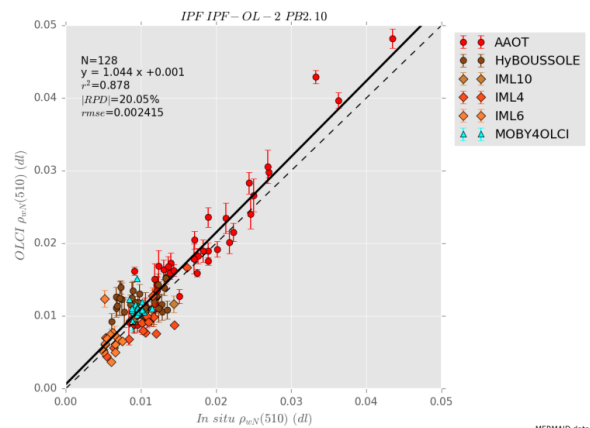
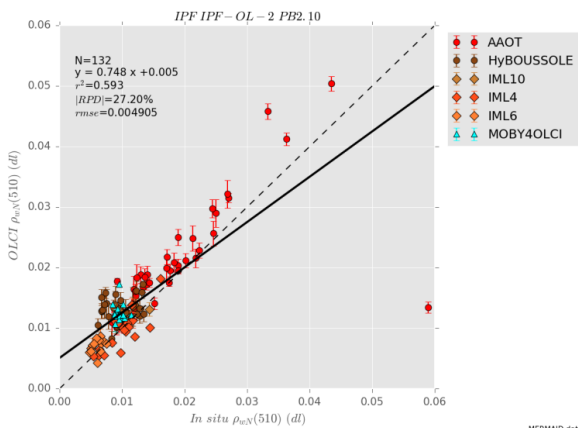
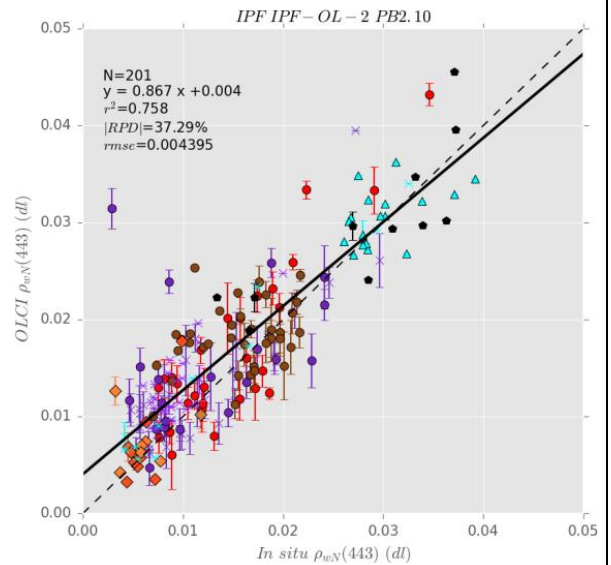
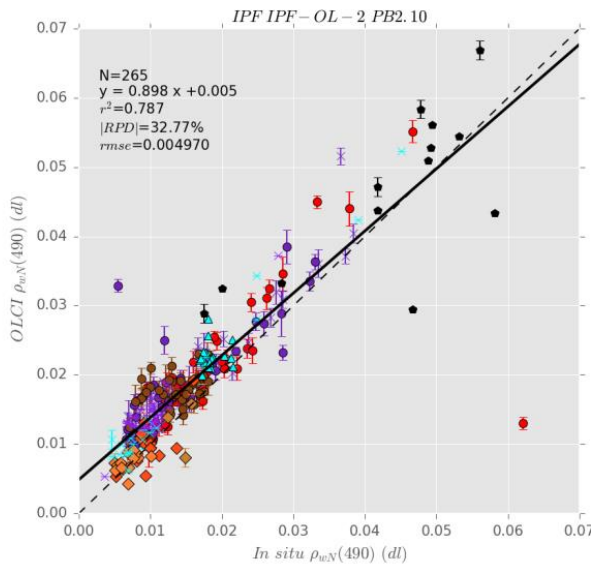
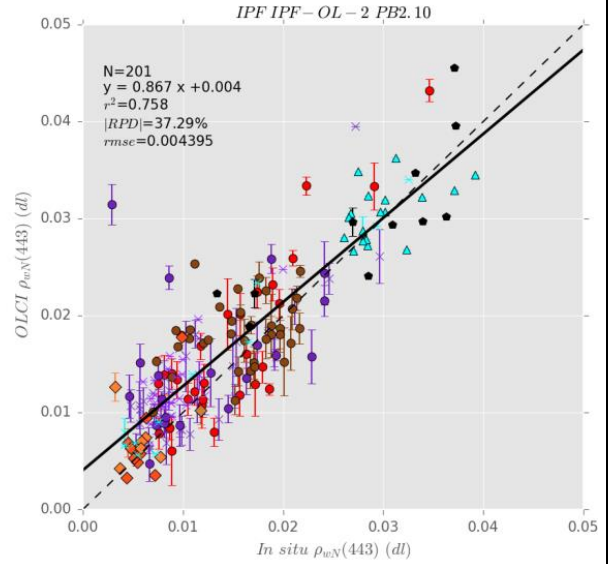
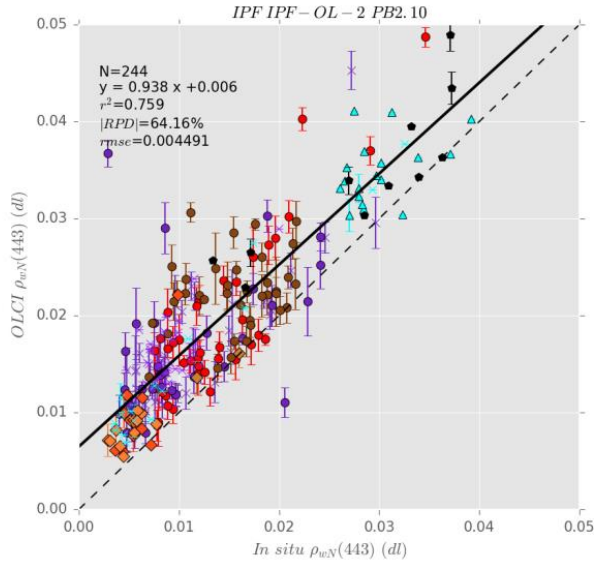
The overall effect of vicarious calibration is two remove the bias observed on marine reflectance therefore significantly reducing the relative errors at all bands. The comparison for the same dataset is presented below.





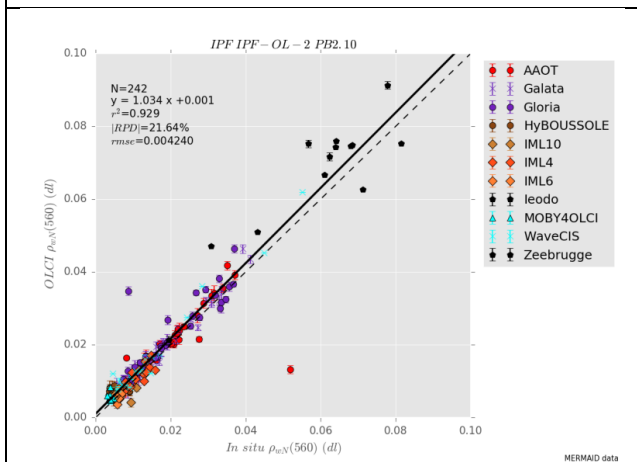
Nominal processor

Vicarious Calibration

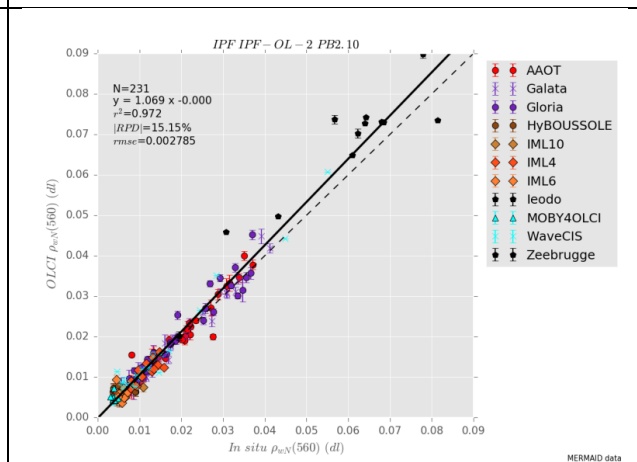




Nominal processor



Vicarious Calibration



	<b>Sentinel-3 MPC</b> <b>S3-A OLCI Cyclic Performance Report</b> <b>Cycle No. 017</b>	Ref.: S3MPC.ACR.PR.01-017 Issue: 1.0 Date: 24/05/2017 Page: 43
--	---	---

## 5 Level 2 SYN products validation

### [SYN-L2-CV-100]

There has been no update on SYN products validation quantitative assessment during the cycle. Last figures (cycle 10) are considered valid.

Qualitative assessment by product inspection showed no detectable performance evolution.

	<b>Sentinel-3 MPC</b> <b>S3-A OLCI Cyclic Performance Report</b> <b>Cycle No. 017</b>	Ref.: S3MPC.ACR.PR.01-017 Issue: 1.0 Date: 24/05/2017 Page: 44
--	---	---

## 6 Events

Three OLCI Radiometric Calibration Sequences have been acquired during Cycle 017:

- ❖ S01 sequence on 27/02/2017 12:39 to 12:41 (absolute orbit 5372)
- ❖ S01 sequence on 12/03/2017 08:38 to 08:40 (absolute orbit 5555)
- ❖ S01 sequence on 22/03/2017 14:21 to 14:23 (absolute orbit 5701)

	<b>Sentinel-3 MPC</b> <b>S3-A OLCI Cyclic Performance Report</b> <b>Cycle No. 017</b>	Ref.: S3MPC.ACR.PR.01-017 Issue: 1.0 Date: 24/05/2017 Page: 45
--	---	---

## 7 Appendix A

Other reports related to the Optical mission are:

- ❖ S3-A SLSTR Cyclic Performance Report, Cycle No. 017 (ref. S3MPC.RAL.PR.02-017)

All Cyclic Performance Reports are available on MPC pages in Sentinel Online website, at:  
<https://sentinel.esa.int>

***End of document***